nature portfolio

Peer Review File

Foaming Photopolymers as a High-Resolution Biomimetic Printing Platform

Corresponding Author: Professor Easan Sivaniah

Any redactions in this file are there to maintain patient confidentiality, the confidentiality of unpublished data, or to remove third-party material.

This file contains all reviewer reports in order by version, followed by all author rebuttals in order by version.

Version 0:

Reviewer comments:

Referee #1

(Remarks to the Author)
Summary of the key results
The manuscript reports a “deep foam photolithography” (DFP) approach to generate polymer foams by UV exposure in the presence of a photoinitiator and a weak solvent. The authors demonstrate that this process can create volumetric foamed structures with strong scattering and structural colour, and that it can be spatially patterned to yield regions of differing porosity and wettability. The work further presents bio-inspired comparisons to natural foams and tissues, as well as microfluidic demonstrations that exploit the patterned wetting properties and flow control in channels fabricated on these foamed substrates.
Overall, the concept and some of the demonstrations are visually compelling, and the combination of foaming, structural optical effects and wettability patterning is interesting. However, as it is written now, the manuscript reads somewhat like two partially separate stories: the core DFP method and associated optics/wetting physics (which could stand on its own as a strong, focused paper), and a suite of downstream microfluidic and “designer liquid” demonstrations that are less conceptually novel and are not yet mechanistically underpinned to the same depth.

Originality and significance
The basic idea of using a photolithographic foaming process for structurally white/coloured and wetting-patterned polymer films is interesting and potentially original. However, the work currently feels split between a core methods/optics story and a secondary microfluidics story, with the latter adding less conceptual novelty. Claims of generality and “nature’s best” benchmarking seem stronger than what is solidly demonstrated. Also previous work by Hölscher and Vignolini and colleages sets a certain precedence on using foams for color.
Data and methodology
Important experimental details and mechanistic explanations are missing or only briefly treated, especially the exact foaming mechanism, collapse, and the 3D structure of the foams (particularly for the strongly scattering and structurally coloured samples). The structural analysis is too limited for a work centred on structure–optics–wetting relationships. The material choices (e.g. PC) are not clearly justified relative to more commodity polymers, which weakens claims of broad applicability. Several figure panels are under-discussed or interpreted in a way that feels ahead of the data.
Most importantly, the mechanism of foaming and the resulting internal structure are not characterised in enough depth. For a process that relies on micro- to meso-scale porosity to produce whiteness and structural colour, a full structural analysis would be highly valuable. In the current version, it is difficult to assess pore size distributions, connectivity, gradient formation and how these depend on exposure, solvent, or polymer. Three-dimensional structural characterisation (for example via tomography or 3D confocal imaging) would be especially important for the structurally coloured and/or strongly scattering white samples.
As mentioned above, some material choices also raise questions about general applicability. For example, the use of polycarbonate (PC) is technically interesting but relatively expensive and less “commodity” than, say, polystyrene (PS) or other common thermoplastics. This choice should be better justified, and the claim of broad applicability would be strengthened by more extensive data on widely used, lower-cost polymers.

Appropriate use of statistics and uncertainties

Reproducibility, number of replicates, and error treatment are not clearly described for key measurements (optical spectra, contact angles, time-dependent wetting, microfluidic performance). For such heterogeneous foams, a clearer statement of variability and uncertainty would be important, particularly for contact-angle and angle-dependent optical data, but also for structural measures.

Conclusions: robustness and validity
The main conclusion that DFP enables biomimetic, structurally coloured and highly scattering foams with spatially programmable properties is plausible but, in my view, not fully substantiated as presented. The mechanistic picture of how foaming initiates, evolves and collapses, and how this relates quantitatively to the structural and optical properties, remains incomplete. The conclusions should more closely reflect what is directly shown, and clearly separate demonstrated results from speculation.

Suggested improvements
The manuscript would benefit from a tighter focus on the DFP mechanism, structure and optics/wetting, with microfluidic demonstrations streamlined or better justified. A more complete structural characterisation (ideally 3D or depth-resolved) of the key foams, clearer explanation of the foaming and collapse process, and better-documented surface roughness and wetting measurements would significantly strengthen the work. If broad material generality is claimed, more commodity polymers should be included or the scope of claims reduced. Angle-resolved data are needed if “iridescence” is claimed; otherwise, the terminology should be adjusted. Clarify the nature of structural colour and any iridescence.

References
The introduction and discussion under-cite important work on polymer foams (including NIPS), structural whites and disordered scattering media, and UV-induced behaviour in specific polymers. Many general statements are not referenced. The reference list and contextual discussion should be expanded so the work is properly positioned within the existing literature (for example, including work such as 10.1002/adma.201702057 on whiteness optimisation via FDTD). I understand that that is a downside of the Nature format, but I would still urge to add more references.

Clarity and context
The abstract and introduction are too short to provide adequate context and do not clearly state what is genuinely new relative to previous approaches. Some wording is imprecise or overstated (e.g. polymers “having a spectrum” or “altitude”, “nature’s best”). Clarifying key terms (foams vs spongy tissues, structural colour vs iridescence) and expanding the introduction to reflect the state of the field would improve clarity.

Line-by-line and figure comments
• L 26–30: Differentiation between foams and spongy tissues is unclear; please define terms and clarify why the distinction matters.
• L 37: A polymer does not “have a spectrum”; rephrase to refer to the measured optical spectrum of a film or sample.
• L 39: “Altitude” of what? A polymer does not have an altitude; the term is confusing and should be replaced or clarified.
• L 41–50: Introduction is too short and not representative of the global research field; expand and add key references on foams, structural whites/colours, and biomimetic optics.
• L 70: Statement lacks reference; specify temperature and give a supporting citation.
• L 71–76: Several claims here need references; please add appropriate citations.
• L 81: Collapse is mentioned but not clearly shown; either show it explicitly or adjust the wording.
• L 84: The cited refs focus on PS and specific UV behaviour; do not present this as universal for all polymers without further support.
• L 94: Title is unclear; please rephrase so the meaning is obvious.
• L 117–134: Interpretation appears too strong; Figs. 2d,e are not discussed in order or in enough detail. Please expand and align text with the figure panels.
• L 139: Specify how surface roughness was measured (instrument, parameters).
• L 140: Provide references for the properties/behaviour of the counterpart materials used.
• L 143: The connection made here is not well explained; add more explanation of the underlying reasoning.
• L 152: References for NIPS are missing; these are necessary given the established literature.
• L 158 and Fig. 3: Clarify whether the colour is truly iridescent (angle-dependent) or angle-independent structural colour. If iridescence is claimed, explain how it was measured and show angle-resolved data.
• L 171: PMMA is not generally expected to show strong scission under typical UV; please verify and support with data or references, or revise.
• L 174: “PC has 90°” is unclear; rephrase and integrate into the text so the meaning (e.g. contact angle) is explicit.
• L 180: The process described sounds like breakout crystallisation or a related transition; please explain the mechanism more clearly.
• L 204: Justify why measurements were performed in the IR and how this relates to the main conclusions.
• L 213: Please discuss prior work such as 10.1002/adma.201702057, which used FDTD to optimise whiteness, and add other relevant refs on structural whiteness.
• L 223ff: This section is hard to follow; clarify the aim of these experiments and what is concluded from them.
• L 277: Rationale for “designer” solutions in microfluidic tests is unclear. Why not use water alone? Please justify the choice.
• L 280: “Recommend” (or the wording used here) is unclear in context; rephrase.
• Figure 2: “Nature’s best” in the caption/label feels overstated and not essential; consider moderating or explaining.
• Figure 3: Untreated contact angles need better discussion. The straight line above 4000 s appears unrealistic; when droplets bounce, assigning 180° contact angle is not appropriate. Angles should be taken in static or quasi-static conditions.

• Figure 6: Please specify what material was used.
• Extended Data Figures 2 to 7: Scale bars are unclear; ensure all scale bars are clearly visible and labelled with units.

Referee #2

(Remarks to the Author)
The authors presented a very interesting and clever method to novel biomimetic printing process that emulates natural hierarchical foam structures in polymer films using spatially patterned UV illumination and a weak solvent to precisely control nucleation, expansion, and collapse of micro-foams within polymer layers, achieving up to 20,000 DPI resolution. And furthermore, the resulting structures show strong light scattering like beetle scales, high aspect ratio foam morphologies, tunable wettability (superhydrophobicity), and interconnected porous networks for microfluidics.
The hierarchically rough surfaces itself is very interesting and it will have diverse application areas. However, this research is a bit premature for publication and lacks deeper physics explanation and concrete evidences in a current state. And I wonder if the results can be reproduced by other researchers. More detailed information on the experiment needs to be provided. I am sure the authors may improve this paper after addressing the following comments. I am looking forward to see the revised version.
1) Firstly, the authors assume a solvent front moving by case II diffusion, given the evidently strong interaction of the polymer with the solvent. Secondly, at early times, we find that the mean bubble diameter D scales approximately as D~t (see Fig. 2c), consistent with an osmotically driven bubble growth with progressive transport of solute into the bubble preventing solute dilution6. Assuming film thickness scales with bubble number and size, we predict a film growth that scales with Δh(t)~t^2. How does the film growth scale with t^2? Is this simply the bubble diameter is proportional to time? If so, the thickness had better be more related to volume (which is proportional to t^3)? More detailed calculation logic needs to be provided for this film growth prediction.
2) The individual traces correspond to development at different temperatures, with lower UV dosage at the lowest development temperature: the broad agreement in the curves is a result of the scaling of time and growth height by their respective values at t_b, the time taken for the front to reach the base of the film (Supplementary Note 2). This reflects the importance of front migration in determining growth rate in the first regime. What does the 'front' mean in "the time taken for the front to reach the based of the film"? Does the front mean the top face of the expanding film or the front of moving solvent?
3) As shown in figure 2b, sequential nucleation with front migration is highlighted by looking at a scatter plot of bubble diameter D vs. depth at different times. At earlier times, the slant in size vs. depth shows that bubbles tend to be smaller at greater depths, since they have had less time to grow than those nucleated near the surface. The physical meaning of figure 2b is hard to understand. The physical meaning of the dotted lines at different times, the locus of deepest bubbles, locus of shallowest bubbles need to be provided.
4) When longer development times and lower molecular weights are used, films can undergo multiple morphological changes following film growth, which may include a reduction in height (Fig. 3a, b), formation of microparticles (Fig. 3c, d), and an increase in surface roughness. Films with lower molecular weight are more plastic than their high molecular weight counterparts; structural evolution is faster, so there is still a significant amount of solute as the bubbles reach large sizes. The combination of hypotonic pressure and the thinning of the walls lead to yielding of the film, rupture of the walls, and collapse of the film
5) The evolution of the foam structure with development time can be visualized in a typical whitening process: optimal whiteness is reached at earlier times but fades as the foams become larger than the required range for visible Mie scattering, as shown sequentially in Fig. 1c. What is the optimal whiteness? How can it be defined or measured? And what is the required range for visible Mie scattering? They should be further defined.
6) The light scattering ability of DFP regions compare favourably with best-in-class performance in nature seen in the white scales of two species of beetles, as well as recent synthetic realizations of structural white. Is there any reference such as paper, book etc?
7) Figure 2 shows the growth and light scattering properties of DFP films. The graphs ((a) Change in thickness over time for foamed 192-kDa polystyrene films, where triangle, circle and square denote development at 22°C (2000 J cm-2 dose), 32°C (3000 J cm-2 dose), and 62°C (3000 J cm-2 dose), (c) Mean diameter of 76 largest bubbles, and number of bubbles per micrometre of film width over development time for foamed 192-kDa polystyrene film, (d) Transport mean free path of 810 nm light in foamed 192-kDa polystyrene films over development time, and (inset) thickness normalized by as-illuminated film) should provide the error bar or statistical information.
8) A key feature of DFP domains is how strongly they scatter light. To gauge the light scattering ability of the films independent of their thickness, a transport mean free path (lt) at a wavelength of 810 nm from the transmission and thickness of the films was derived as shown in Fig. 2d. There is a strong reduction as the pores grow to sizes where they effectively scatter visible light, followed by an increase as they grow even larger. The reduction of opacity for long development times is also evident in Fig. 1c. As height continues to grow with time under these conditions, a similar correspondence can be seen between lt and film height. For the thin film, there are usually optical standing wave inside the film to make craze-like microfibrils like the authors did previously (Nature, 570, 363–367 (2019)). Does the similar phenomena happen in this study? If not, why not?
9) The bubble growth kinetics underlying film expansion was considered by measuring growth exponents of the change in film height Δh as a function of time, as shown in Fig. 2a. SEM cross-sections for the data sets are given in Extended Data Figs. 2 to 4. How was the film height measured? Was it measured for the same sample or different samples? If it was measured for the same sample sequentially, I wonder how the vacuum environment in SEM measurement affect the sample formation.
10) A schematic is given in Fig. 3a, and growth height over time is given in Fig. 3b. Corresponding SEM cross-sections with

thickness time series are given in Extended Data Fig. 5 to 7. Film failure begins near the top of the film, where the bubbles become largest and the walls are thinnest. This leads to bubble rupture and subsequent relaxation, which reduces the film height. How can the largest bubble and thinnest wall be predicted? Are they known only by measurement, can not be predicted?
11) The authors mentioned that with long exposure under certain conditions, microparticle formation can be seen with a brilliant iridescence, as shown in Figs. 3c, d. Figure 3a shows 'microsphere' in amorphous. Is the 'microparticle' same with the 'microsphere'?
12) Hierarchically porous structure is a very useful material with the multiscale structure in the same material from nano to microscale. They have been used for other applications such as bioinspired radiative cooling devices (Nanoscale Horizon, 7, 1054 (2022)), energy devices (Adv. Funct. Mater., 22, 4634, (2012)), sensors, displays and etc. They can be further discussed for potential applications of the development.
13) The authors discussed that under long enough exposure and development, it was expected that the skin layer to also fail, exposing the inner structure of the foam. Combined with patternability of foam regions, this lends itself to localized modification of roughness, and thus permeability and hydrophobicity/hydrophilicity. From the observation from the authors, exposing the inner structure of the foam seems to be related to the hydrophobicity/hydrophilicity. The hydrophobicity/hydrophilicity is usually predicted by Wenzel or Cassie-Baxter model. The authors are suggested to use those models to predict the hydrophobicity/hydrophilicity.
14) The foam structure, both pre- and post-collapse, becomes decorated with needle-like nanostructures protruding from bubble walls. They start isolated (Fig. 3e) but continue to grow with development time into larger features with extended needles (Fig. 3f). The function of the 'microflower' is not clear for current DFP film. Do they only affect the roughness and hydrophobicity/hydrophilicity? Are they related to other characteristics such as optical, mechanical or chemical characteristics of DFP film?
15) Exposure was also achieved using light sources with different wavelength ranges and power levels, including both monochromatic and broad-band illumination. Broad-band light sources were also effective in DFP foam formation. DFP foam formation was verified using a mercury lamp equipped with an optical filter (λi: 350-405 nm, Contact Mask Aligner, MA/BA8 Gen3, SÜSS MicroTec), and a standard LED flood lamp (λi: 395–405 nm AR-UV1-100W, Shenzhen Huanpin Testing Technology, Co., Ltd.), respectively. I wonder why monochromatic and broad-band illumination as well were effective. Does this mean the careful wavelength selection is not important for successful DFP foam formation?
16) For the practical application, scale-up manufacturing for a large area is very important. Current study was demonstrated for a relatively small area. A large-area LED array was custom-ordered from Micro Square Co., Ltd (λi : 365, 385, and 405 nm). For each wavelength, 12 × 54 bulbs were assembled in a rectangular arrangement with 1-cm spacing between bulbs along both the width and length. The irradiance of the LED array was linearly adjustable from 0 to 750 mW cm^{-2} at a working distance of 10 cm, corresponding to the range of the power adapter output. What is the limiting factor for a large area scale up? How can this limitation be overcome?

And there are many more comments. I will continue the comments when this paper can go to the next review stage.

Referee #3

(Remarks to the Author)
In their study, Easan Sivaniah and co-workers introduce deepfoam photolithography, which is a versatile strategy to locally impart porous structures within surface-near regions of thermoplastic substrates. In the presence of radical photoinitiators, the authors exploit (UV) light-mediated chain scission/crosslinking processes to change polymer-solvent interactions. Once photopatterned, the films are immersed in acetic acid acting as weak solvent and the solvent uptake leads to a volume expansion of the film. Depending on the development time and the exposure conditions, the films undergo various changes in their morphology such as a reduction in height, an increase in surface roughness or regular microparticles are formed on the samples' surface. The hierarchically structured morphologies lead to a change in optical properties and high resolution patterns with varying colors are generated. The conceptional approach is similar to a previous study of the authors (https://doi.org/10.1038/s41586-019-1299-8), which exploits solvent-induced stress crazing to form microfibrils and cavities in thermoplastic films. In the current work, they significantly advance the process by being able to create porous structures with different morphologies over varying length scales. Along with optical properties, the change in morphology also promotes a local control in surface wettability over an extended range, even reaching superhydrophic characteristics due to the hierarchical architecture of the formed structures.
From a chemistry viewpoint, the process impresses with its simplicity and might be easily extended to other light sources emitting light at longer wavelengths by adding other types of radical initiators (e.g. near IR light to activate radical initiators and generate chain scission in even deeper regions). By offering the possibility to spatially control the morphology of porous structures, the work is relevant for numerous application fields and is expected to be highly appealing for the readers of Nature. The manuscript is well written but lacks some studies on the underlying chemical mechanisms and thus, I would recommend that the manuscript requires a revision.
Major issue:
(1) The authors thoroughly studied the physical aspects of the foaming process including evolution of the porous structures and foam morphologies as a function of various parameters (e.g. exposure dose, development time, etc.). However, the chemical change (crosslinking versus chain scission) in the network has to be also addressed to better understand the foam dynamics. It's recommended that the authors include contrast curves (plotting soluble or gel fraction versus exposure dose) of the studied materials.
Minor points and questions:
(2) How do mechanical or thermal properties of the thermoplastic substrates (prior to swelling) change due to the light-triggered chemical processes?

(3) How critical is the drying time of the swollen networks? How is the foam morphology affected by the evaporation kinetics of the solvent?
(4) In the conclusion section, the authors state that foaming is possible over the entire volume. However, this is true only for very thin films. It's recommended that the authors rephrase this statement accordingly.
(5) The photoinitiator content is rather high (several experiments were carried out with films containing 9 wt% of the photoinitiator), which is expected to comprise on the penetration depth of the incident light (internal filter effect). Were the porous structures only obtained in films containing a higher photoinitiator content? If this is the case, it would be interesting to compare contrast curves of thermoplastic substrates with varying photoinitiator contents.

Version 1:

Reviewer comments:

Referee #1

(Remarks to the Author)
The revised manuscript presents a substantially improved and more coherent version of the original submission. The authors have clearly taken the reviewers' comments seriously and have significantly strengthened both the mechanistic understanding and the overall focus of the work.

Most importantly, the mechanistic aspects of the DFP process are now much better developed. The addition of 3D FIB-SEM analysis, confocal imaging of the solvent diffusion front, and photochemical characterization (GPC, FTIR, and TGA) provides a much clearer picture of the underlying processes governing pore nucleation, growth, and collapse. The identification of a case-II diffusion front and the discussion linking solvent permeation, chain scission, and foam formation substantially clarify the physical basis of the process - and lay the foundation for interesting followup work.

The structural characterization has also been improved, particularly through the combination of FIB-SEM analysis, optical transmittance measurements, and mechanical characterization using nanoindentation. These additions help establish a more convincing relationship between the evolving foam structure and the resulting optical and mechanical properties. The use of transport mean free path to contextualize the structural whiteness of the material relative to natural and biomimetic systems is a useful addition. It might be useful to cite the relevant literature to whiteness in discussion on page 5 a bit more.

I also appreciate that the authors have streamlined the manuscript by reducing the emphasis on the microfluidic demonstrations. While I still think this aspect could be left out for a follow-up paper altogether, leaving it in like this feels ok.

All in all, a nice revision!

Referee #2

(Remarks to the Author)
Qin and colleagues responded very well to the reviewers' comments. Even though my previous comments were really quite extensive, the authors carried out a lot of backup experiments and characterizations to successfully provide the direct evidences for the conclusion and added sound discussions. I am well satisfied with the first revision and favorable to the publication of this research results. I found that some of my previous comments are similar to the comments from other reviewers and most of them were answered satisfactorily.
Although the authors cleared up most of the important issues, there are still some remaining issues need to be addressed in further revision. To improve the quality of this research, I want to check one more review round. Here are the detailed issues needing attention,
1) Most of the discussions and new results were very useful and insightful. I am sure they will greatly strengthen the novelty of this study. However, some of them were just discussed in the rebuttal. They had better be briefly mentioned in the main manuscript or at least in the supporting information especially the new experiments and characterization requested in the first revision round.
2) The authors very well answered the reviewers' request for depth of understanding by conducting 3D analysis and photochemical analysis to clarify the dynamics and chemical driving forces behind the DFP foaming process, both during foam growth and collapse, as well as identifying the conditions whereby a foam could be stable, or collapse. And furthermore they broadened the concept of DFP by demonstrating that it could be applied equally to the 2D geometry of a fiber, generating the DFP printing of structural white and patterned wettability in fabrics. The DFP in fiber looks very interesting. However, it is still not well understood why the authors added fiber results.
3) In response to my previous comments on case II diffusion, it is great to provide the direct evidence of a case II diffusion front of the developing solvent, acetic acid with the 3D FIB-SEM image in Figure 2a. It is also interesting to see the presence of a nucleation zone of foam behind this front, from which microphases of solvent and UV scission products nucleate and grow. However, the colors in the figure are a bit confusing cause the color is kind of randomly assigned. How about use the color according to the size of the bubbles to show the size distribution in the real FIB-SEM images?
4) DFP is a light induced foaming process where a photosensitized polymer film is exposed to a deeply penetrating UV-A light, which initiates the production of both scission and cross-linked polymers throughout the depth of the film. A weak solvent was used to develop the DFP foam structure. The solvent permeates into the film and bubbles of solvent/scission-product rich domains are formed which nucleate, grow, and coalesce, resulting in a closed, foam-like cellular microstructure. When the UV-A light is irradiated onto the thin film, there can be light interference to form a stack of intense-weak layers. I

wonder if there is any interference effect that was previously observed in reference 47 in the polymer thin film.
5) Usually, polymer thin films suffer from the crazing problem under large deformation (bending and strain). Especially, polystyrene suffers from whitening under repeated deformation. Cycling bending causes micro-structure change in polymer film. This will be very important for the actual applications. In this study, exposure is not limited to planar films. An example is shown in Fig. 5i, where a pattern has been applied to a curved poly(2-hydroxyethyl methacrylate) (PHEMA) contact lens dip-coated with polystyrene and thioxanthone. Other examples of printing on bendable substrates like polypropylene sheets are given Extended Data Fig. 8(d,e,f,g). The intricate DFP patterns are preserved after the release of acute bending. The long-term cycling acute bending test should be carried along with the cross-sectional SEM pictures to check if there is any micro/nano scale change during the bending. If there is any micro/nano scale change in the DFP film, it will change the micro structure of DFP and thus deteriorate the performance of the DFP film.
6) Microfluidic fluid control usually uses inner channel for the fluid transport. However, current microfluidic uses the control of fluid flow on patterned surfaces where the effect is strong enough that a droplet passed over unexposed regions can detach small volumes from the main droplet to form isolated liquid domains (Fig. 6a, also Supplementary Movie). This may not only be applied to the controlled delivery of analytes in parallelized lab-on-a-chip applications, but also to the control of fluid flow on patterned surfaces. However, very small volumes of fluid flowing on the surface (or even closed pores that are exposed on top) will evaporate very fast. This may mean the fluidic control can not be used for the large area sample, which will not be enough useful for the microfluidic applications because the fluid properties (such as concentration, composition etc) will continuously changes and becomes unpredictable. This critical issue needs to be further discussed.
7) Alternatively, single “pixels” may be exposed which realize highly localized foam regions. This can be used to print dithered images with high precision. An example produced using microLED exposure is shown in Fig. 5c along with a higher magnification microscope image of the underlying dithering in Fig. 5d. SEM images of these individual foamed regions (Fig. 5e) reveals strong localization of the foaming; the resolution achieved is 20,000 dpi. What is the limiting factor for this high resolution?
8) Usually, polymer films suffer from the poor stability at low temperature. Usually, polymer thin film becomes very brittle at low temperature and factures into pieces. Fig. 5a (in the previous paper) shows a time lapse of a DFP pattern exposed to air at reduced temperature; droplets condense selectively on unexposed, less hydrophobic regions, where they are also more prone to coalescence. I wonder if the DFP film has enough mechanical stability under low temperature.
9) Figure 5 f shows the angle-dependent colour of the printed image of The Girl with a Pearl Earring, placed on a human finger, printed by microLED illumination. Insets are the same sample with slight rotations. Fig. 5f shows a grating type ‘Vermeer’ image printed; tilting yields different diffractive colors. Periodic grating structures with slightly different relative spacings can be combined with structural white to create an ‘SDG’ logo specimens featuring both diffractive 40 colour and structural whiteness. The angle information should be indicated in the picture and the scale bar is missing in this picture.
10) Figure 5 shows various images generated by current technology including (b) a greyscale printing of the photo Albert Eistein using UV projector (c) printing a dithered image of the Mona Lisa by micro-LED illumination, (f) angle-dependent colour of the printed image of The Girl with a Pearl Earring, placed on a human finger, printed by microLED illumination etc. For the printing applications, this technology should be demonstrated for a large size. What is the largest size and what are the limiting factors for scale-up?
11) Continuing the previous comment, the uniformity will be prime factor for the high quality printing. How is the uniformity of the scale-up sample? The uniformity can be defined in terms of pore size, size distribution, thickness, color etc. Additionally, the discussion on the primary factor decides the uniformity and the potential solution can be further discussed.
12) The mechanisms by which DFP domains scatter light, repel water, and transport fluids are all readily found in nature. White beetles remain a key benchmark for structural white, a bar met by DFP domains; water repellency by hierarchical roughness is driven by the same dewetting physics behind the lotus effect. The authors put the picture of white beetles in several pictures including Figure 1(b), Figure 3(d), Figure 5(b). However, it is a bit distractive to show them in many pictures. It can be seen in a separate figure in Figure 3(d) while the beetle in Figure 1(b), Figure 5(b) had better be removed.
13) There are still some digital pictures (Extended data Figure 3) and drawings missing scale bars. They should be added to the pictures.
14) Some letters in some figures (figure 2C) are too small to read. They should be enlarged for enhanced visibility.
15) For the respond to previous comments on the material combination dependence, the authors carried out various backup experiment for various materials. DFP domain formation depends only on plasticity, hypotonic permeation, and crosslinking; beta scission in the presence of oxygen and crosslinking due to reaction between sites on the polymer radicalized by hydrogen abstraction are common mechanisms to a wide range of commercial polymers. Hence we show that the DFP process is also broadly applicable to a range of commercially available polymers including polycarbonate (PC) and polyethylene terephthalate (PET) using a range of photoinitiators (see Extended Data Fig 6). Besides the pictures in the extended data, if the authors can provide a table summarizing the material candidate, it will be helpful to the readers.

Referee #3

(Remarks to the Author)
The authors have addressed all recommendations and questions satisfactorily. The included contrast curves at different photoinitiator concentrations have strengthened the discussion and conclusions of the work. Thus, publication of the manuscript in its current form is recommended.

Version 2:

Reviewer comments:

Referee #2

(Remarks to the Author)
I carefully read the responses to the comments and I found most of the issues were well addressed. Especially, the scale-up demonstration was very impressive beyond my expectation. I do not need to review this paper again but it will be great if the authors can further provide the quantitative information on the uniformity of the DFP printing especially at large size for the response to my previous comments (10),(11) because the scale-up may deteriorate the uniformity of the print.
I really enjoyed reading every line of this paper and now I am totally satisfied with the response from the authors and fully support the publication of this research.

For Attn of reviewers :

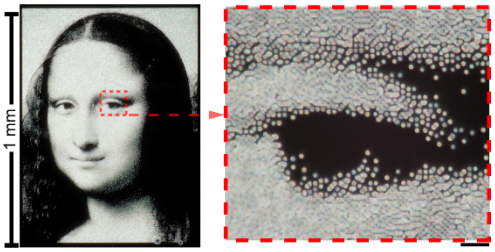

Thank you for your supportive review of our paper; every single reviewers' response was deeply insightful, prompting several interesting new experiments to consolidate our initial understanding of the DFP process. To briefly remind you:

DFP (DeepFoam Photolithography) is a light induced foaming process where a photosensitized polymer film is exposed to a deeply penetrating UV-A light, which initiates the production of both scission and cross-linked polymers throughout the depth of the film. A weak solvent (acetic acid) is used to develop the DFP foam structure. The solvent permeates into the film and bubbles of solvent/scission-product rich domains are formed which nucleate, grow, and coalesce, resulting in a closed, foam-like cellular microstructure. We took advantage of the DFP process in two broadly different ways; (a) we used the light scattering ability of foams in amorphous polymers to realize high-resolution printing of structural white; (b) we created patterned superhydrophobicity within the collapsing foam of a semi-crystalline polymer.

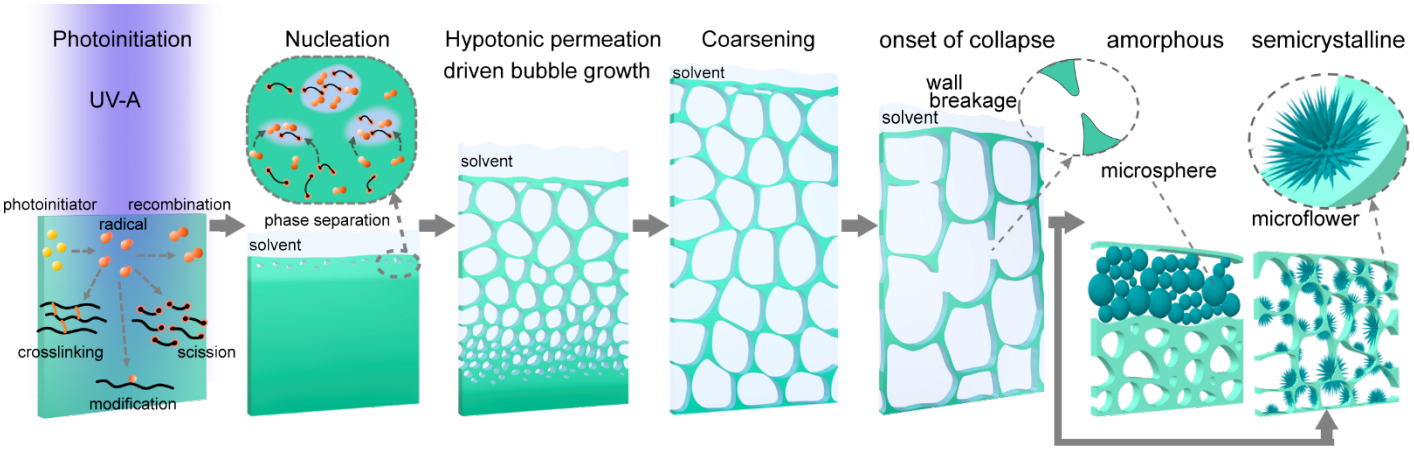

We found the reviewers' comments incredibly constructive to the point that major improvements were made in the last 3 months, adding significant depth and breadth to the manuscript.

(1) Specifically, we answered the reviewers' request for depth of understanding by conducting 3D analysis and photochemical analysis to clarify the dynamics and chemical driving forces behind the DFP foaming process, both during foam growth and collapse, as well as identifying the conditions whereby a foam could be stable, or collapse.
(2) We broadened the concept of DFP by demonstrating that it could be applied equally to the 2D geometry of a fiber, generating the DFP printing of structural white and patterned wettability in fabrics.

Through these improvements, we feel certain to have at least identified what key physical principles are at work within the entire DFP process. It should provide a suitable framework for future research either through quantitative modelling of the process or optimizing the outcomes of the process for practical applications.

To improve the clarity of our response letter, the highlights of these improvements are summarized first. All major additions to the text and figures are provided addressing those improvements, referred to as **Revision Text 1–10**. Finally, a line-by-line response to each reviewer's comments are given, specifically referencing **Revision Text 1–10**, and any additional minor textual additions. We do so to avoid repeating the revised text, when indeed there are many common suggested improvements by the reviewers.

Highlights

The unanimous request of the reviewers was a clarification of the growth mechanism of DFP. This has now been done through Focused Ion Beam electron microscopy (right) to reveal the underlying 3D-structure forming process, and GPC, FTIR, and confocal microscopy and spectrophotometry, to address the photochemical and kinetic aspects of the work. The deeper study confirmed the following:

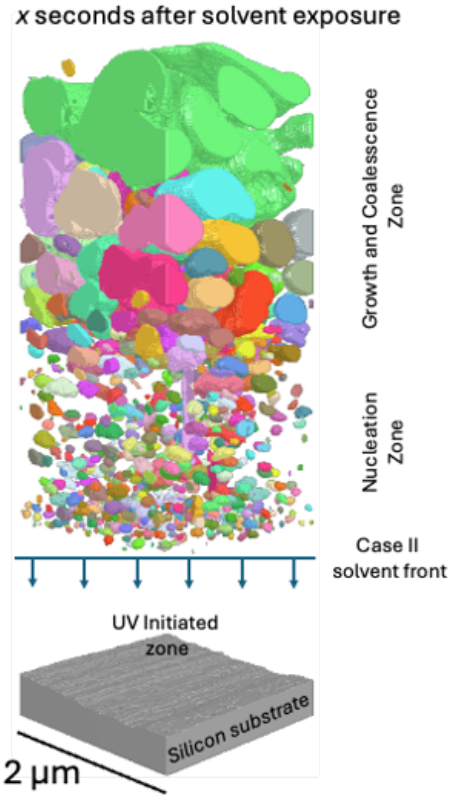

- A case II diffusion front of the developing solvent, acetic acid, was directly observed. It also revealed the presence of a nucleation zone of foam behind this front, from which microphases of solvent and UV scission products nucleate and grow. (**Revision Text 1,2**)
- A quantitative structure-property relationship of the foaming process was made for both structural whiteness and mechanical strength of the foam. The former drew comparisons to significant works in the biomimetic field (**Revision Text 3**), whereas the latter drew upon an elegant validation of the seminal Gibson-Ashby model for cellular materials. The same mechanical data was used to identify the viscoelastic response of the foamed film during collapse (**Revision Text 3, 4**).
- Contrast curves indicated that all combinations of polymer molecular weight and photoinitiator have the capability to foam, but the likelihood of stable expansion or collapse was determined by the relative amount of photochemically generated scission products and cross-linked materials **(Revised Text 5).**
- Besides polystyrene and polycarbonate, we highlighted the material generality of the DFP process to common amorphous and semi-crystalline polymers by demonstrating its printing and foaming structures in polyethylene terephthalate (PET), PMMA, cellulose triacetate (CTA), and polysulfone. **(Revised Text 6)**
- Detailed roughness analysis using AFM and X-ray diffraction analysis revealed the importance of breakout crystallization during the foaming and collapse of semi-crystalline polycarbonate. The resulting needle-like protrusions were found to be essential for realizing enhanced hydrophobicity (**Revision Text 7**).
- Importantly, we extended the DFP principle from a planar to a cylindrical geometry by achieving foam-like structures in polystyrene fibers in a non-woven fabric. By extension, DFP printing on polycarbonate fibers led to patterned superhydrophobic fabrics. With this demonstration, the plausibility of achieving DFP in 3D colloids increases immensely as does the capability to cross-over from film-making and coatings to various material manufacturing processes. (**See Revision Text 8**)

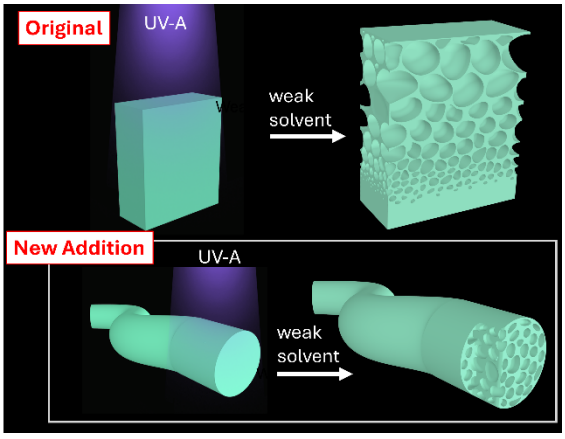

- Further improvements to clarity are described in **Revision Text 9,10**, especially regarding the creation of diffractive color, the minimization of our coverage of DFP microfluidics (which could be a future work), and reducing the inclusion of speculative contributions (such as transient structural color).

Detailed explanation of revisions

Whereas all of what follows is within the paper, we explain key additional data that improve the manuscript, followed by a line-by-line response to each reviewer's comments, to address specific queries on the original manuscript. To avoid double explanations, all replies presented in this response letter primarily consist of quoted text (in Times Roman, Ft 10, Italics, blue) from the modified manuscript. The reviewers' original comments are in (Green, Arial, Ft. 10)

The mechanism of DFP formation and growth.

Revision Text 1.

An overview of the mechanism for DFP growth was generated by conducting 3D FIB-SEM analysis of the foam during its nucleation and growth phase. We find evidence for a case II diffusion front of solvent traversing the film depth, creating a nucleation zone of pores behind it. We recommend that the reviewers also examine Supplementary Movie 1. (refers to 25 sec data shown below) as an example of a original FIB SEM Sequence prior to its machine-learning assisted analysis of porosity shown here.

Focused Ion Beam-SEM (FIB-SEM) analysis of the same films reveal an identical trend. 3D rendering of individual pores shows a front of pores moving towards the glass substrate, growth in pore size, and subsequent film expansion (Extended Data Fig. 3 and Supplementary Movie 1). However, whilst this 3D analysis has quantitative limitations due to ion-beam damage, more subtle details in the DFP process are revealed. Analysis of bubble size with depth relative to the top of the film during early solvent permeation (see Fig. 2a) reveals a region just above the permeating solvent front which contains a sharp distribution of small (< 100 nm) pores. These are highlighted in different colours for the three earliest development times in the scatter plot, both in pore size and depth distributions (see Fig. 2b). The permeation front clearly moves faster than successful nucleation can occur, leaving a metastable region where isolated heterogeneous nucleation sites or spontaneous fluctuations yield pre-critical bubble nuclei; hence the critical nucleation size for subsequent growth ~100nm. Closer to the top surface, successfully nucleated bubbles have entered a growth phase and are larger, as they have had more time to grow.

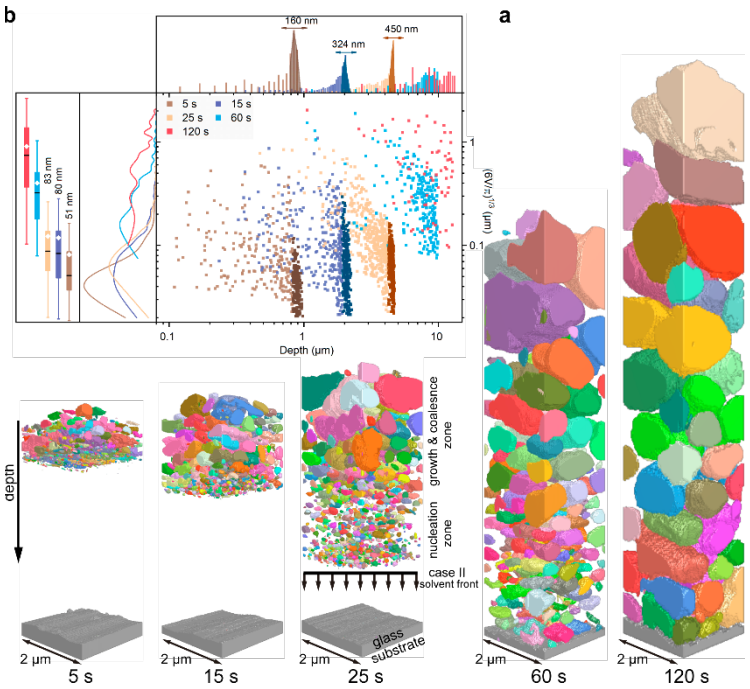

Revision Text 2.

The existence of a case II diffusion front was directly identified using confocal microscopy, and its kinetics measured via spectrophotometry. Diffusion rate is correlated to the UV-induced chain scission kinetics determined from GPC.

Whereas the 3D FIB-SEM intimates the existence of a diffusing solvent front, we can directly identify it through in-situ 3D confocal microscopy by fluorescently labelling the polymer film and developing solvent bath (Fig. 2c and Extended Data Fig 4a–c). The linear reduction over time in thickness of the initial polymer slab clearly shows a case II diffusion dynamics5 (Supplementary Figs. 1–4 and Supplementary Note 1). From a GPC analysis of molecular weight in UV exposed polymer (Fig. 2d, Supplementary Figs. 5–8 and Supplementary Note 2), we find that enhanced UV exposure leads to a greater number of scission events (N_s). The confocal-

laser derived case II diffusion velocity also increases with irradiation time (Fig. 2e); an increase in scission products induces a higher hypotonic potential for solvent permeation.

In-situ reflectance studies allow efficient sampling of the initial speed of the case II front in the first few seconds of solvent entry prior to light-scattering pore formation (Extended Data Fig. 4d–i and Supplementary Note 1). In agreement with the confocal-observed case II diffusion results, the front velocity and solvent fraction (ϕ_2) can be resolved as a function of molecular weight, temperature and irradiation (Fig. 2e). A direct comparison of velocities across molecular weights is speculative, since the relative amounts of scission products, and the degree of cross-linking are both molecular weight dependent. However, identical molecular weight and irradiation at different temperature reveals a simpler picture of faster case II diffusion and greater swelling with solvent (ϕ_2) at higher temperatures.

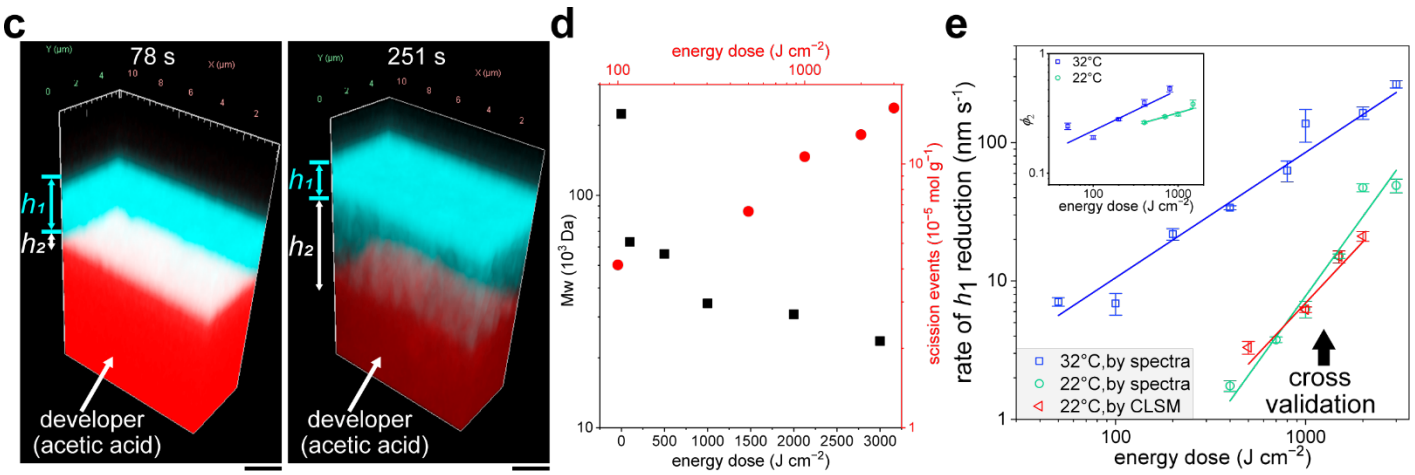

Revision Text 3.

Foam growth was correlated to directly observable optical metrics (Transmittance).

To gauge light scattering ability of the films independent of their thickness, we measured the total transmittance of the films over a wide range of wavelengths (Fig. 3c inset). For demonstration, we specifically plot transmittance at 810 nm (Fig. 3c). There is a strong reduction as the pores grow to sizes where they effectively scatter visible light, followed by an increase as they grow even larger. Due to this coupling between pore size and light scattering ability, different wavelengths have transmittance minima at slightly different times. From such transmission data, we can derive a transport mean free path (l_t) at a wavelength of 810 nm from the transmission and measured average porosity of the expanded films (Fig. 3d, Supplementary Note 5, Supplementary Fig. 11.) Calculation of l_t as a measure of structural whiteness, as well as the use of simulations to benchmark the interaction of biomimetic structures with light[7–9] helps us gauge the optical scattering efficiency of DFP foams within a common framework. We consider l_t and the film thickness of three examples of DFP films compared to a range of different systems in the literature, as shown in Fig. 3d (also Supplementary Note 6). Similar mean free paths are achieved with significantly thinner films than in two species of white beetle, Cyphochilus spp. and Lepidiota stigma, both considered benchmarks for structural white.

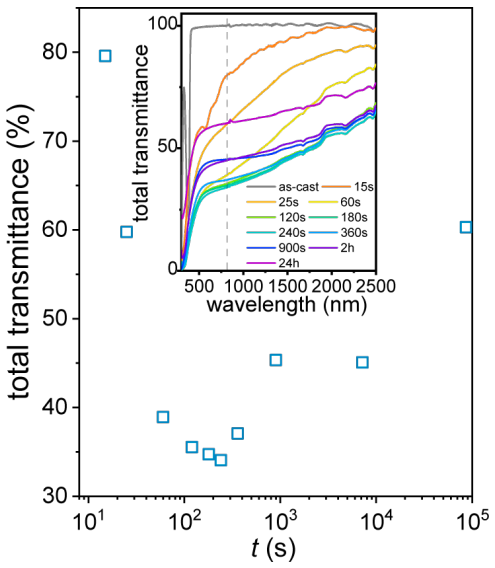

Revision Text 4.

Foam growth and the dynamics of collapse were correlated to directly observable mechanical metrics.

(a) In stable foams:

DFP foams have a characteristic elastic response which provides an independent measure of how physical structure changes with development time. Nanoindentation measurements of the Young's modulus were taken for films at different development times (Supplementary Note 7 and Supplementary Fig. 12). We use the seminal Gibson-Ashby model[10] for elastic response, and calculate a porosity ϕ, assuming most of the elasticity comes from the foam edge structure, not compression of the thin films separating adjacent pores. The Young's modulus of the foam is given by $E=E_s(1-\phi)^2$, where E is the measured modulus, E_s is that of the polymer, and ϕ is the porosity or volume fraction of the pores. We compare the derived porosity with those derived from FIB measurements and the change in thickness (Supplementary Note 7). All these methods yield consistent results, as shown in Fig. 3e for expanded foams.

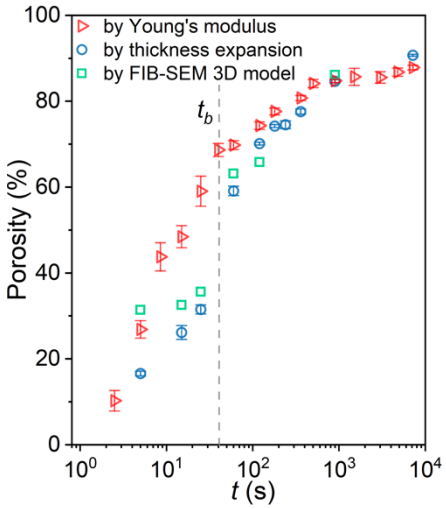

(b) In collapsed foams:

We again consider porosity derived from nanoindentation measurements, as shown in Fig. 3g. Here, instead of a plateau, film collapse corresponds to a decrease in porosity. This is consistent with the above picture: when films rupture, surrounding walls relax and retract in response to imbalanced forces. The walls become thicker, and the porosity decreases, with the Young's modulus (and porosity) evolving towards the original solid film state. Note that with long exposure under certain conditions, aggregates and colloid formation can be seen below the skin layer, as shown in Extended Data Fig. 5 and depicted in Fig. 1c. These aggregates are transient and appear to be washed out over longer development times (Supplementary Fig 15).

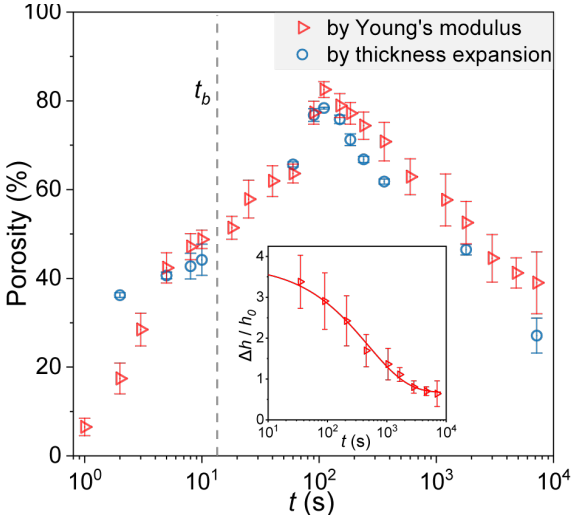

While DFP domains strongly resemble liquid foams, many of the driving forces governing rupture and retraction clearly do not apply, such as drainage and droplet formation[11–13]. We analyse the change in film height with development time since the initiation of collapse; due to their availability and consistency with measurements from SEM cross-sections, we derive heights from nanoindentation measurements. A viscoelastic response by the film is expected upon film rupture, given the presence of both chain scission and crosslinking in these films. As shown in the inset of Fig. 3g, the height relaxation is fit well by a Kohlrausch-Williams Watt (KWW) stretched exponential Fig. 3g (inset)[14]. The KKW relationship best describes dynamical heterogeneity in arrested systems, especially typical of a viscoelastic entangled polymeric network with a broad spectrum of relaxation times (see Supplementary Note 7).

Revision Text 5.

We carried out photochemical analysis to confirm scission and cross-linking. Photolithographic contrast curves were also measured to identify stability conditions for foams.

DFP begins by selectively exposing a polymer film containing a photoinitiator to patterned light. In exposed regions, radicals are produced which trigger chain scission and crosslinking in the polymer network[3]. The well-known pathways for a film of PS[15,16] and the photoinitiator THX are recalled (Supplementary Note 2) and confirmatory experiments discussed there. Briefly, Attenuated Total

Reflectance Fourier Infrared Spectroscopy (ATR-FTIR) confirmed the formation of carbonyl bonds due to main chain scission upon irradiation; in Fig. 2d, we showed an increasing fraction of low molecular weight products with greater energy dosage. Thermogravimetric analysis (TGA) corroborates this through an increasing fraction of the original mass dissipated at lower temperature but also reveals a high molecular weight fraction (too high for GPC) which increases with dosage.

DFP is only possible when there is enough scission product to drive hypotonic permeation and phase separation, but requires a mechanically rigid crosslinked network to support the foam structure; these are elements of positive and negative photoresists. We may gauge this balance by measuring the equivalent of a photoresist-like contrast curve in PS-THX films (Fig. 3h, Supplementary Note 2). This set of curves, for a full range of irradiation times, and THX concentrations, indicates the percentage of (cross-linked) material that remains after development. For a classical positive photoresist, this fraction will always trend to zero at long enough irradiation times; this is clearly seen in the low molecular 35kDa PS curves. The trend is also seen in higher molecular weight PS curves, but these require a greater THX content to drive accelerated scission. As the figure indicates, foaming is mechanically stable so long as the proportion of scission products makes up the minority component of the irradiated film composition.

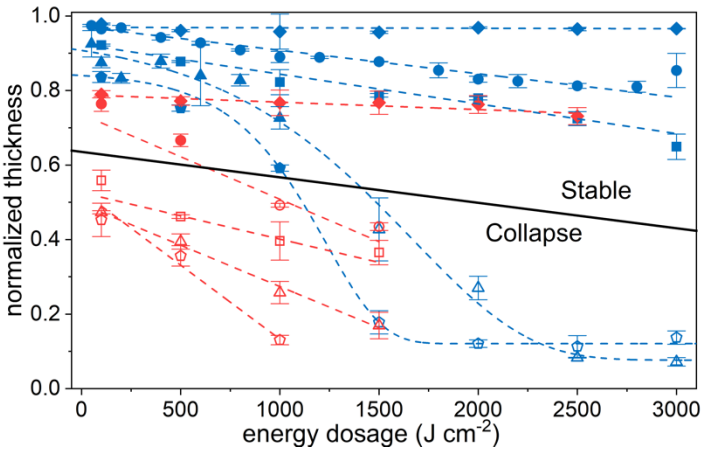

Revision Text 6.

Extension of DFP to other polymers (semi-crystalline, amorphous commodity plastics).

DFP domain formation depends only on plasticity, hypotonic permeation, and crosslinking; beta scission in the presence of oxygen[17] and crosslinking due to reaction between sites on the polymer radicalized by hydrogen abstraction[18] are common mechanisms to a wide range of commercial polymers. Hence we show that the DFP process is also broadly applicable to a range of commercially available polymers including polycarbonate (PC) and polyethylene terephthalate (PET) using a range of photoinitiators (see Extended Data Fig 6). DFP is clearly also possible in semi-crystalline materials, where that intrinsic property adds functionality to the foam structures.

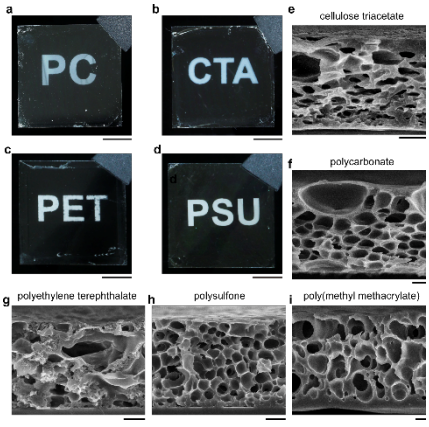

Revision Text 7.

The role of microflower lateral roughness, breakout crystallization, and microflower structures were clarified in their contribution to superhydrophobicity.

Semi-crystalline polycarbonate followed the same stages of foaming and collapse as in 35-kDa polystyrene. Interestingly, the foam structure, both pre- and post-collapse, becomes decorated with isolated needle-like nanostructures protruding from bubble walls (see Fig. 4a and 4b). They grow with development time into larger features with extended needles (Fig. 4c) that engulf the originally rough structure (Fig. 4d). These "microflowers" have been documented for flat semicrystalline polymer films, including polycarbonate, when treated with a volatile solvent[19,20]. X-ray diffraction on these films (Supplementary Fig. 16), reveals peaks consistent with crystallized domains that grow with development time; we can conclude that this is a form of breakout crystallization

at the surface. The appearance and growth of these features during the DFP process is consistent with enhanced plasticity due to chain scission.

The appearance of microflowers during collapse lends to hierarchical roughness, consisting of fine, needle-like features at the lowest scale and the collapsing foam structure at higher scale. The difference this makes to its wetting behaviour can be seen when roughness and contact angles are compared between polystyrene (35kDa) and polycarbonate (45kDa). Root-mean-squared (RMS) roughness is determined using atomic force microscopy (AFM) (Supplementary Note 8 and Supplementary Fig. 17). After film collapse, both show a surface roughness which grows and plateaus with development time, as shown in Fig. 4g. The plateau roughnesses are similar in both systems. In the context of Cassie-Baxter wetting, this should yield a similar evolution in contact angle, since the contact area would be similar. However, in polycarbonate, Fig. 4g shows that contact angle rises drastically to above the threshold for superhydrophobicity[21]. This is consistent with direct comparison of SEM cross-sections of collapsed polycarbonate and 35-kDa polystyrene foams (see Extended Data Fig. 7). The decoration of the roughened structure with microflowers clearly plays a vital role in determining wetting properties. The general spatial distribution of microflower structures (from PC) and hence capacity to be superhydrophobic likely to be function of initial film volume.

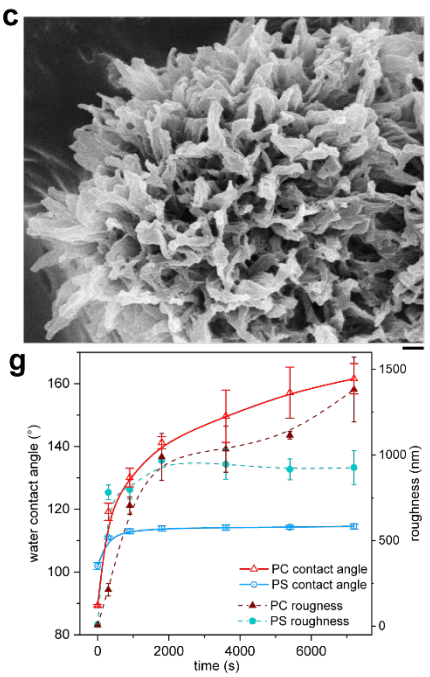

Revision Text 8.

Extension of DFP to 2D fibers

(a) for printing porosity into fabrics:-

Both polystyrene and polycarbonate can be spun[22] into fibers. We demonstrate the DFP process electrospun fabrics of polycarbonate and polystyrene fibers (Fig. 5j, Supplementary Note 9, and Supplementary Fig. 20). For polystyrene, in addition to THX, the fibers optionally also contained a dye to initially create a blueish fabric. These showed the same sequence of surface-initiated pore formation seen in flat films, as shown in Extended Data Fig. 9. Fig. 5k shows a foamed cross-section of multiple fibers within a DFP developed fabric. In bulk, DFP fabric exhibits strong light scattering (Fig. 5l), mimicking the light scattering quality of polar bear fur.

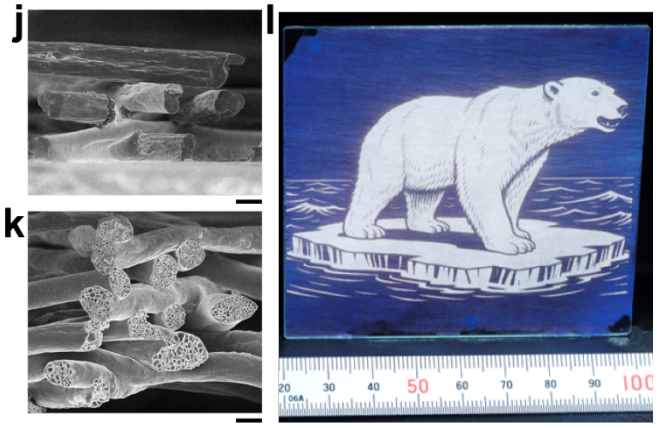

(b) for printing wettability into fabrics - A polar bear image is selectively wet with colored water :

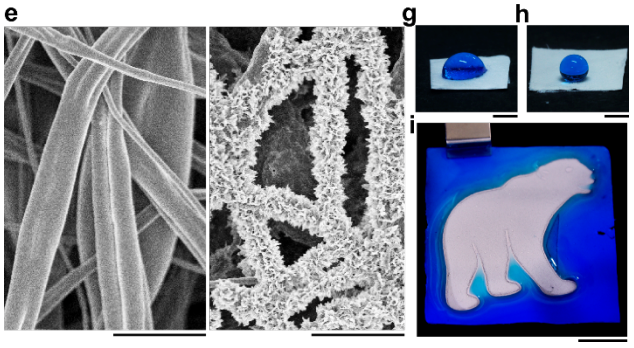

Smooth electrospun fabric of polycarbonate fibers containing THX photoinitiator (inset Fig. 6e) develop the same dense microflower structure through the DFP process (Fig. 6e and 6f); coverage is both uniform and complete. The fabrics gains a superhydrophobic character from this surface morphology (Fig. 6g, h). The same patterned wettability and confinement effects seen for printed films can be realized on woven surfaces; Fig. 6i and Supplementary Fig. 21b shows the same demonstration of selective dip-coating. The ability generate superhydrophobic fabrics offers a PFAS-alternative and a potential to realize low-cost microfluidics and analysis devices[26].

Revision Text 9

Other minor adjustments:

(a) The effect of drying time: in revision, we added Supplementary Fig. 22. which included the following brief text, understandable in the context of the main document.

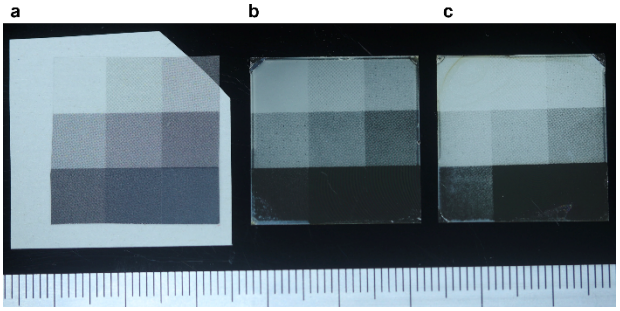

Supplementary Fig. 23 | Effect of different drying methods. a, Greyscale overhead projector (OHP) mask (background is a piece of A4 paper for contrast). b, DFP film dried using an air blower immediately upon the completion of development. c, DFP film dried via natural solvent evaporation. Ruler for scale (cm). 2.5-μm-thick polystyrene (192 kDa) was spin-cast on cover glass using a solution containing 7 wt% of thioxanthone relative to polymer. The film was illuminated using a custom LED chamber (Thorlabs λ_i: 385 nm) with an energy dose of 500 J cm^{-2}. A greyscale OHP sheet consisting of a 3×3 grid display is used as the photomask: an 8-bit greyscale gradient ascending from 0 (bottom-right) to 255 (top-left) in uniform numerical increments. The illuminated films were developed in 32 ℃ acetic acid for 20 s. The sample dried via natural solvent evaporation is more opaque than one dried immediately using an air blower. This result indicates the effect of drying on the resultant DFP films: the longer the developer (acetic acid) remains in the film, the more development continues to happen.

(b) Angle-dependent iridescence in printed DFP structures: in revision, we demonstrate angle-dependent change in the color (now re-named diffractive color instead of iridescence) in the printing of regularly spaced DFP pixels.

Alternatively, single "pixels" may be exposed which realize highly localized foam regions for high precision dithering. An example produced using microLED exposure is shown in Fig. 5c and 5d, along with a higher magnification SEM image in Fig. 5e. Strong localization gives resolutions of up to 20,000 dpi, high enough to accurately print angle-dependent diffractive features for visible light. Fig. 5f shows a grating type 'Vermeer' image printed; tilting yields different diffractive colors. Periodic grating structures with slightly different relative spacings can be combined with structural white to create an 'SDG' logo specimens featuring both diffractive colour and structural whiteness, as shown in Fig. 5g and Supplementary Fig. 19.

Revision Text 10

Omissions in revision.

(a) Microfluidic applications: we significantly reduced the discussions and figure panels on microfluidics, leaving the full development to a future paper, and only introducing the idea by a single example. Furthermore, the example of selective condensation on superhydrophobic patterns was entirely removed, for interests of space, and considering that the effect was easily inferable.

Prior to film collapse, we note that the pores in the cell structure below the skin layer are not entirely intact. This enables the transport of liquid through foams via capillarity; as a simple example, an ethanol/water mixture containing a fluorescent dye is drawn into the features of complex porous root-pattern created by DFP in polystyrene, as shown in Fig. 5h, inset, and Extended Data Fig. 8. Organic liquids can primarily be drawn by capillarity into these hydrophobic channels; further development of DFP into hydrophilic materials is needed to transfer this concept into the mainstream of pump-free high resolution, microfluidic applications.

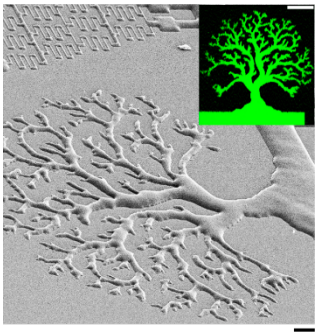

(b) Discussions on the iridescence arising from complex intermediate collapse morphologies: In revision, we feel that the feature, although reproduceable, is a transient property that was not yet completely controlled and its origins could only be speculated on; hence the observation of such structural color features were removed in the main manuscript, but noted within the supplementary section.

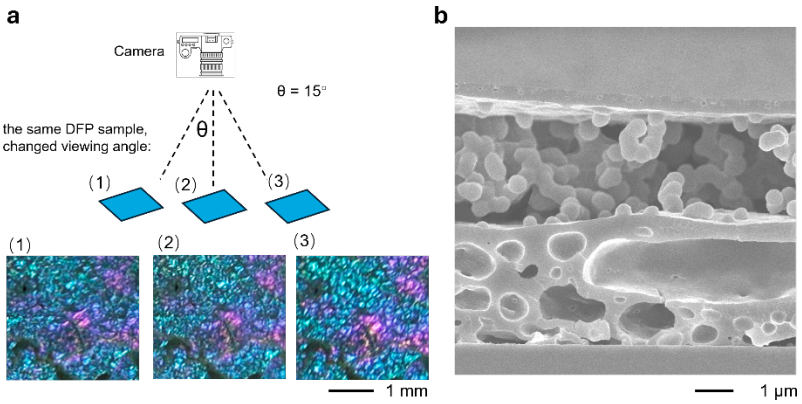

Supplementary Fig. 15 | Structural colours observed in the collapsed DFP films containing microspheres. a, Structural colours of a collapsed 35-kDa polystyrene (PS) film observed with different viewing angles. b, SEM cross-sectional image of the collapsed 35-kDa PS DFP film. Scale bars, 1 mm (a); 1 μm (b). 2.7-μm-thick PS (35 kDa) film with 5 wt% thioxanthone content relative to PS was cast on a cover glass slip, illuminated using a custom LED chamber (Thorlabs, λ_i: 385 nm) with an energy dose of 2000 J cm^{-2}, and developed in 22 ℃ acetic acid for 25 s. Structural colours related to microsphere formation show colour consistent with a certain range of viewing angle (±15). However, it is worth noting that such structures are transient and appear to be washed out over longer development times. Elucidation of the formation mechanism for this particular morphology, and how it relates to its apparent iridescence, is left for future work.

Line By Line response to Reviewers

Referee #1 (Remarks to the Author):

Summary of the key results

The manuscript reports a "deep foam photolithography" (DFP) approach to generate polymer foams by UV exposure in the presence of a photoinitiator and a weak solvent. The authors demonstrate that this process can create volumetric foamed structures with strong scattering and structural colour, and that it can be spatially patterned to yield regions of differing porosity and wettability. The work further presents bio-inspired comparisons to natural foams and tissues, as well as microfluidic demonstrations that exploit the patterned wetting properties and flow control in channels fabricated on these foamed substrates.

Overall, the concept and some of the demonstrations are visually compelling, and the combination of foaming, structural optical effects and wettability patterning is interesting. However, as it is written now, the manuscript reads somewhat like two partially separate stories: the core DFP method and associated optics/wetting physics (which could stand on its own as a strong, focused paper), and a suite of downstream microfluidic and "designer liquid" demonstrations that are less conceptually novel and are not yet mechanistically underpinned to the same depth.

Originality and significance

The basic idea of using a photolithographic foaming process for structurally white/coloured and wetting-patterned polymer films is interesting and potentially original. However, the work currently feels split between a core methods/optics story and a secondary microfluidics story, with the latter adding less conceptual novelty.

We have taken this recommendation on board; given the significant addition to our mechanistic understanding of the DFP process and its extensions into cylindrical geometries, the microfluidic demonstration is limited to a conceptual introduction. Generally, the DFP structures tend toward hydrophobic materials, and the microfluidic application would have more impact once we generated similar structures in hydrophilic materials (work in progress).

The DFP mechanism is now described in depth in the **Revision Texts 1 to 5**. Please also refer to **Revision Text 10a** for modification to microfluidics section.

Claims of generality and "nature's best" benchmarking seem stronger than what is solidly demonstrated. Also previous work by Hölscher and Vignolini and colleages sets a certain precedence on using foams for color.

We have taken steps to address previous work by researchers (Holscher and Vignolini and others) who have created a vital framework on structural color and white materials, whereas references to "nature's best" have been rephrased to refer to "natural benchmarks" for structural white.

The DFP process unifies diverse approaches to the modification of polymer films. Photolithography is merged with phase separation driven foam structuration resembling NIPS. It should be noted that techniques like NIPS are widely used to make highly scattering porous membranes (as reviewed[28,38]), while biomimetic approaches to highly scattering films have also been explored, characterizing both natural[7,9,39–42] and artificial[8,43–46] films with a disordered internal structure.

Data and methodology

Important experimental details and mechanistic explanations are missing or only briefly treated, especially the exact foaming mechanism, collapse, and the 3D structure of the foams (particularly for the strongly scattering and structurally coloured samples). The structural analysis is too limited for a work centred on structure–optics–wetting relationships. The material choices (e.g. PC) are not clearly justified relative to more commodity polymers, which weakens claims of broad applicability. Several figure panels are under-discussed or interpreted in a way that feels ahead of the data.Most importantly, the mechanism of foaming and the resulting internal structure are not characterised in enough depth. For a process that relies on micro- to meso-scale porosity to produce whiteness and structural colour, a full structural analysis would be highly valuable. In the current version, it is difficult to assess pore size distributions, connectivity, gradient formation and how these depend on exposure, solvent, or polymer. Three-dimensional structural characterisation (for example via tomography or 3D confocal imaging) would be especially important for the structurally coloured and/or strongly scattering white samples. (Please see **Revision Texts 1 to 3.**)

As mentioned above, some material choices also raise questions about general applicability. For example, the use of polycarbonate (PC) is technically interesting but relatively expensive and less "commodity" than, say, polystyrene (PS) or other common thermoplastics. This choice should be better justified, and the claim of broad applicability would

be strengthened by more extensive data on widely used, lower-cost polymers. (Please see **Revision Text 6** for Generality to commodity polymers.)

Appropriate use of statistics and uncertainties

Reproducibility, number of replicates, and error treatment are not clearly described for key measurements (optical spectra, contact angles, time-dependent wetting, microfluidic performance). For such heterogeneous foams, a clearer statement of variability and uncertainty would be important, particularly for contact-angle and angle-dependent optical data, but also for structural measures. (Please see **Line-by-Line response** below)

Conclusions: robustness and validity

The main conclusion that DFP enables biomimetic, structurally coloured and highly scattering foams with spatially programmable properties is plausible but, in my view, not fully substantiated as presented. The mechanistic picture of how foaming initiates, evolves and collapses, and how this relates quantitatively to the structural and optical properties, remains incomplete. The conclusions should more closely reflect what is directly shown, and clearly separate demonstrated results from speculation. (Please see **Revisions Texts 3 and 4** for structure-property relationships)

Suggested improvements

The manuscript would benefit from a tighter focus on the DFP mechanism, structure and optics/wetting, with microfluidic demonstrations streamlined or better justified. A more complete structural characterisation (ideally 3D or depth-resolved) of the key foams, clearer explanation of the foaming and collapse process, and better-documented surface roughness and wetting measurements would significantly strengthen the work. If broad material generality is claimed, more commodity polymers should be included or the scope of claims reduced. Angle-resolved data are needed if "iridescence" is claimed; otherwise, the terminology should be adjusted. Clarify the nature of structural colour and any iridescence.

The reviewers comments and suggestions for improvement have been so significant that the large amount of text, revised text and new data was added (See **Revision Texts 1-10**). A primary concern of reviewer #1; a lack of fundamental structure-development analysis is now addressed in **Revision Texts 1 to 5**, which include a description of the DFP mechanism starting from photochemical initiation (**Revision Text 5**), connection between structure and optics (**Revision Text 3**), new 3D FIB-SEM measurements (**Revision Text 2**), and 3D confocal microscopy investigation of early permeation (**Revision Text 2**). We also add AFM measurements of roughness (**Revision Text 7**) compared to changes in wetting angle, which highlight the role played by microflower formation in polycarbonate. Broader generality is evidenced by SEM sections of DFP in different materials (**Revision Text 6**). Regarding iridescence, we have reframed this in terms of "diffractive color", since the color is generated by printing gratings using the DFP technology (**Revision Text 9b**). Moreover, we have now generated an understanding for what combination of polymer molecular weight/photoinitiator/irradiation energy will eventually collapse (**Revision Text 5**) and a viscoelastic nature of the collapse dynamics (see **Revision Text 4b**).

References

The introduction and discussion under-cite important work on polymer foams (including NIPS), structural whites and disordered scattering media, and UV-induced behaviour in specific polymers. Many general statements are not referenced. The reference list and contextual discussion should be expanded so the work is properly positioned within the existing literature (for example, including work such as 10.1002/adma.201702057 on whiteness optimisation via FDTD). I understand that that is a downside of the Nature format, but I would still urge to add more references.

Clarity and context

The abstract and introduction are too short to provide adequate context and do not clearly state what is genuinely new relative to previous approaches. Some wording is imprecise or overstated (e.g. polymers "having a spectrum" or "altitude", "nature's best"). Clarifying key terms (foams vs spongy tissues, structural colour vs iridescence) and expanding the introduction to reflect the state of the field would improve clarity.

The reference list is now nearly doubled and includes context of a general framework for characterizing structural white, as given above. Clarity and contextualization of our finding amongst previous attempts to use porous structures for their light scattering properties is now addressed primarily through an extended discussion and conclusions since there are certain limitations on abstract length. Nonetheless we have improved the accuracy of the abstract :-

Nature creates a diverse range of foam-like materials, from bones to banana peels, through a rich orchestration of physical and biochemical processes across hierarchical length scales. Here, we introduce DFP (DeepFoam Photolithography), a spatially controlled, light induced foaming process where a photosensitized polymer film is exposed to a deeply penetrating UV-A light, which

initiates the production of both scission and cross-linked polymers throughout the depth of the film. Hypotonically-driven case II permeation of a weak solvent triggers pore nucleation, expansion, and a controllable viscoelastic collapse to create foams through a localized solubilization of polymer fragments within a cross-linked network. The resemblance to amorphous structural whites in nature enables inkless printing in white and greyscale; the resolution is high enough (~20,000 DPI) to generate diffractive color. This uniquely allows the printing of mechanically expanded and collapsed foams with significant aspect ratios (20x); controlled collapse can create hierarchically rough surfaces with lotus-like super-hydrophobicity. DFP can be applied to both films and fibers, using a range of amorphous and semi-crystalline polymeric materials. Patterning micron-level spatial differences in foamability, wettability, optical properties, and local thickness enable high-resolution printing, microfluidics, as well as picoliter capture of liquids and colloidal matter.

Line-by-line and figure comments

• L 26–30: Differentiation between foams and spongy tissues is unclear; please define terms and clarify why the distinction matters.
We removed "spongy tissue", which we agree is highly non-specific.

• L 37: A polymer does not "have a spectrum"; rephrase to refer to the measured optical spectrum of a film or sample.

Now changed to : "*a wide **range** of polymeric materials*"

• L 39: "Altitude" of what? A polymer does not have an altitude; the term is confusing and should be replaced or clarified.

Now changed to "*local film thickness*," referring to local expansion in printed film areas due to foaming.

• L 41–50: Introduction is too short and not representative of the global research field; expand and add key references on foams, structural whites/colours, and biomimetic optics.

We have added some context in conclusions, and also within the specific section on structural white.

The DFP process unifies diverse approaches to the modification of polymer films. Photolithography is merged with phase separation driven foam structuration resembling NIPS. It should be noted that techniques like NIPS are widely used to make highly scattering porous membranes (as reviewed[28,38]), while biomimetic approaches to highly scattering films have also been explored, characterizing both natural[7,9,39–42] and artificial[8,43–46] films with a disordered internal structure.

• L 70: Statement lacks reference; specify temperature and give a supporting citation.
• L 71–76: Several claims here need references; please add appropriate citations.

In revision, L70 was rephrased and appropriately located in the text in revision. Citations on the scattering of foams were appropriately cited.

The evolution of the foam structure with development time can be visualized in a typical whitening process: optimal whiteness is reached at earlier times but fades as the foams become larger than the required range for visible Mie scattering[4], as shown sequentially in Fig. 1b.

4. Vera, M. U., Saint-Jalmes, A. & Durian, D. J. Scattering optics of foam. Appl. Opt. 40, 4210 (2001).

• L 81: Collapse is mentioned but not clearly shown; either show it explicitly or adjust the wording.
This is now addressed by combining all phases of the DFP process into a single introductory figure (Figure 1c), and now described through revised text and the loss in height and mechanical properties in Figure 3f, 3g. (See **Revision Text 4b**)

• L 84: The cited refs focus on PS and specific UV behaviour; do not present this as universal for all polymers without further support.

We have modified this statement to point out that the general phenomenon of scission and cross-linking occurs in many polymer systems, though our current paper focuses in depth on the PS, THX system. We also do show that the DFP concept has the potential to traverse other polymer systems, by demonstrating it in PET, cellulose acetate, PMMA, polysulfone, and polycarbonate. (See **Revision Text 6**)

• L 94: Title is unclear; please rephrase so the meaning is obvious.

"Growth" has been replaced by "Foam Growth Dynamics"

• L 117–134: Interpretation appears too strong; Figs. 2d,e are not discussed in order or in enough detail. Please expand and align text with the figure panels.

Since each stage of the process requires a discussion of both pore size evolution and changes in film height, we must refer to both these figures in this particular order. We have, however, expanded upon the derivation of the scaling in the main text, and left detailed derivation for Supplementary Note 3. We also concur that some of our statements based on evolving polymer glassiness may have been speculative: these have been removed.

• L 139: Specify how surface roughness was measured (instrument, parameters).

We have now added a significant amount of new data on the evolution of surface roughness. Root-mean-squared roughness was evaluated with an atomic force microscope. Details are provided in the Methods section. Please also refer to Revision Note 7.

• L 140: Provide references for the properties/behaviour of the counterpart materials used.

The original statement was that low molecular weight materials are generally more "plastic" than high molecular weight counterparts. This statement was vague, and un-necessary and therefore has been removed in revision.

• L 143: The connection made here is not well explained; add more explanation of the underlying reasoning.

The reference to osmotic fracture growth refers to the similarity between DFP and hypotonic failure, when the excess of a solute drives solvent flow until material failure. We also speculate that the failure of the walls on thinning might be aided by a reduction of yield stress. However, in light of the referee's suggestion that we tone down speculation, we have removed these altogether.

• L 152: References for NIPS are missing; these are necessary given the established literature.

A dedicated paragraph discussing the relationship between DFP and NIPS has been added.

Although both processes result in foams, the DFP process differs from a visually similar poration phenomenon in nonsolvent-induced phase separation (NIPS) process[27–30]. NIPS is a solidification process from a viscous ternary polymer-solvent-nonsolvent system that does not lead to the observed order-of-magnitude expansions seen in DFP. The backflow of the non-solvent plays an active role in determining the dimension and shape of pores[31]. Contrary to DFP, the resulting NIPS macrovoids have an inverted asymmetric structure, where the largest voids are further from the film–liquid interface[32–34].

• L 158 and Fig. 3: Clarify whether the colour is truly iridescent (angle-dependent) or angle-independent structural colour. If iridescence is claimed, explain how it was measured and show angle-resolved data.

(Please refer to **Revision Texts 9b, 10b**). In revision, the only controlled iridescence we claim is for printed diffraction gratings using foamed stripes. The angle-dependence is shown qualitatively by imaging a sample tilted at different angles. Transient iridescence, reported in the original main part of the manuscript, has been moved (Supplementary Fig. 15) but its transient nature noted as a topic to understand and control better within a future work.

• L 171: PMMA is not generally expected to show strong scission under typical UV; please verify and support with data or references, or revise.

In revision we write:

We note that in examples like PMMA, with poor sensitivity to UV-A exposure, the addition of a photoinitiator is essential[53,54].

53. Mita, I., Obata, K. & Horie, K. Photoinitiated Thermal Degradation of Polymers II. Poly(Methyl Methacrylate). Polymer Journal vol. 22 (1990).
54. Carbaugh, D. J., Wright, J. T., Parthiban, R. & Rahman, F. Photolithography with polymethyl methacrylate (PMMA). Semicond. Sci. Technol. 31, 025010 (2016).

• L 174: "PC has 90°" is unclear; rephrase and integrate into the text so the meaning (e.g. contact angle) is explicit.

We have revised the text as below, making the meaning explicit on contact angle measurements.

...However, in polycarbonate, Fig. 4g shows that contact angle rises drastically to above the threshold for superhydrophobicity[21]. This is consistent with direct comparison of surface SEM images of collapsed polycarbonate and 35-kDa polystyrene foams (see Extended Data Fig. 7).

• L 180: The process described sounds like breakout crystallisation or a related transition; please explain the mechanism more clearly.

We have now obtained X-ray diffraction (XRD) data that confirms a rise in crystalline peaks for polycarbonate in these systems (Supplementary Fig. 16). Yes, we do believe that this is an instance of breakout crystallization, consistent with the plasticization of the material by enough short chain segments. (See **Revision Text 7**)

• L 204: Justify why measurements were performed in the IR and how this relates to the main conclusions.

Measurements were taken over a wider wavelength range (300nm – 2.5 microns), which is captures most of the length scale over which pores develop during nucleation and growth. We specifally determine transmission related mean free pathlength (l_t) at 810 nm to ensure a fair comparison with the work by Vignolini et al. (Ref. 9 in the main text), which adopted the same benchmark. We now present a discussion of transmittance at a range of wavelengths, for a fuller discussion of how structure relates to optical properties. (Please see **Revision Text 3**).

• L 213: Please discuss prior work such as 10.1002/adma.201702057, which used FDTD to optimise whiteness, and add other relevant refs on structural whiteness.

Whilst we cannot do full justice to the remarkable works in this area, we added the following to our discussion of optical properties of foams.

... Calculation of l_t as a measure of structural whiteness, as well as the use of simulations to benchmark the interaction of biomimetic structures with light[7–9] helps us gauge the optical scattering efficiency of DFP foams within a common framework.

7. Wilts, B. D. et al. Evolutionary-Optimized Photonic Network Structure in White Beetle Wing Scales. Advanced Materials 30, (2018).
8. Haataja, J. S., Jacucci, G., Parton, T. G., Schertel, L. & Vignolini, S. Topological invariance in whiteness optimisation. Commun. Phys. 6, (2023).
9. Burresi, M. et al. Bright-white beetle scales optimise multiple scattering of light. Sci. Rep. 4, (2014).

• L 223ff: This section is hard to follow; clarify the aim of these experiments and what is concluded from them.

This section was intended as a demonstration that DFP printing could be achieved in any arbitrary geometry such as curved surfaces. In revision, this inspired us to demonstrate the true versatility of the technology by extending from films towards other 2D geometries such as fibers. (See **Revision Text 8**)

• L 277: Rationale for "designer" solutions in microfluidic tests is unclear. Why not use water alone? Please justify the choice.
• L 280: "Recommend" (or the wording used here) is unclear in context; rephrase.

(For L 277,280) Our current realizations of DFP use hydrophobic polymers. Thus, we used non-polar organic solvents instead of water. In response to your earlier suggestions, we have largely relegated microfluidics to a brief overview. The detailed poration mechanisms and fluid flow in these channels have been left for future work (**See Revision Text 10a**)

• Figure 2: “Nature’s best” in the caption/label feels overstated and not essential; consider moderating or explaining.

Thank you, this has been revised, as described above.

• Figure 3: Untreated contact angles need better discussion. The straight line above 4000 s appears unrealistic; when droplets bounce, assigning 180° contact angle is not appropriate. Angles should be taken in static or quasi-static conditions.

We have reviewed our calculation of contact angles, taking angles in quasi-static condition for the droplet that is repelled away from the microflower surface. We added the below description in the caption text of contact angle plot (Fig. 4g).

For the droplets that are finally repelled away from the film surface, water contact angles were recorded when the droplets are pressed most onto the surface (~164°, panel 4 in f).

• Figure 6: Please specify what material was used.

Though description of the microfluidics has been reduced in revision, the material (polystyrene) has now been clarified in the text.

• Extended Data Figures 2 to 7: Scale bars are unclear; ensure all scale bars are clearly visible and labelled with units.

We have added labels to scale bars where possible, and otherwise ensured visibility, with a clear definition in the caption. Indeed, in response to an earlier comment, all data is now adequately qualified in terms of sample number, and the nature of the standard deviations quoted.

Referee #2 (Remarks to the Author):

The authors presented a very interesting and clever method to novel biomimetic printing process that emulates natural hierarchical foam structures in polymer films using spatially patterned UV illumination and a weak solvent to precisely control nucleation, expansion, and collapse of micro-foams within polymer layers, achieving up to 20,000 DPI resolution. And furthermore, the resulting structures show strong light scattering like beetle scales, high aspect ratio foam morphologies, tunable wettability (superhydrophobicity), and interconnected porous networks for microfluidics.

The hierarchically rough surfaces itself is very interesting and it will have diverse application areas. However, this research is a bit premature for publication and lacks deeper physics explanation and concrete evidences in a current state. And I wonder if the results can be reproduced by other researchers. More detailed information on the experiment needs to be provided. I am sure the authors may improve this paper after addressing the following comments. I am looking forward to see the revised version.

1) Firstly, the authors assume a solvent front moving by case II diffusion, given the evidently strong interaction of the polymer with the solvent. Secondly, at early times, we find that the mean bubble diameter D scales approximately as D~t (see Fig. 2c), consistent with an osmotically driven bubble growth with progressive transport of solute into the bubble preventing solute dilution6. Assuming film thickness scales with bubble number and size, we predict a film growth that scales with Δh(t)~t^2. How does the film growth scale with t^2? Is this simply the bubble diameter is proportional to time? If so, the thickness had better be more related to volume (which is proportional to t^3)? More detailed calculation logic needs to be provided for this film growth prediction.

Thank you for pointing this out. Indeed, bubbles (whose volume grows with t^3; their growth contributes to height as t) ; are being nucleated in a region whose height is growing linearly through case II diffusion.; hence $\Delta h(t) \sim t \times t = t^2$. A full derivation is provided in Supplementary Note 3., we have the following text in the revised manuscript.

…We predict the growth exponent by combining case II diffusion of the front with the growth of individual bubbles. Tracking a set population of the largest bubbles in the film (Fig. 3b), the mean bubble diameter initially scales as approximately $\bar{D} \sim t$. *This is consistent with osmotically driven growth with progressive transport of solute into the bubbles, preventing solute dilution in individual pores; similar growth is seen in blisters in thin polymer films[6]. Combining the linear front migration and the growth exponent for bubbles, we predict* $\Delta h(t) \sim t^2$.

2) The individual traces correspond to development at different temperatures, with lower UV dosage at the lowest development temperature: the broad agreement in the curves is a result of the scaling of time and growth height by their respective values at t_b, the time taken for the front to reach the base of the film (Supplementary Note 2). This reflects the importance of front migration in determining growth rate in the first regime. What does the 'front' mean in "the time taken for the front to reach the based of the film"? Does the front mean the top face of the expanding film or the front of moving solvent?

3) As shown in figure 2b, sequential nucleation with front migration is highlighted by looking at a scatter plot of bubble diameter D vs. depth at different times. At earlier times, the slant in size vs. depth shows that bubbles tend to be smaller at greater depths, since they have had less time to grow than those nucleated near the surface. The physical meaning of figure 2b is hard to understand. The physical meaning of the dotted lines at different times, the locus of deepest bubbles, locus of shallowest bubbles need to be provided.

Addressing both of these comments:

(Please see **Revision Text 1, 2**). The 'front' refers to the moving solvent front by case II diffusion moving downwards toward the substrate, ahead of which is pure polymer, and behind which there is an onset of nucleating pores that subsequently grow with more solvent, leading to the expansion of the overall film. We recognize the ambiguity in our original description. Thanks to additional measurements requested by the reviewers, we can identify the front movement directly via confocal microscopy, and indirectly through reflectance studies.

In revision, we also used FIB electron microscopy to study the 3D structure of a developing foam. It showed that until the solvent front reaches the bottom of the film, there is a tightly bunched grouping of nucleating pores formed that develops deeper into the film. This sets an approximate length scale for the nucleation of scission/solvent microphases at ~50-100nm. Once the front reaches the bottom of the sample, running out of material to create more nucleating pores, the pore size largens and its distribution broadens, though simple kinetics dictate that pores nucleated earlier (at the surface

of the film) are larger than those in the bulk.

In revision, we feel the 3D FIB SEM data is a more phenomenologically accurate descriptor of the foaming process ; indeed the observation of a tightly bunched nucleation zone was missed in the original analysis of 2D SEM sections. However, dimensional accuracy is compromised in FIB SEM, due to some inevitable melting during ion-beam milling; hence, the 2D SEM data is retained in the analysis of the growth of the largest pores over time.

4) When longer development times and lower molecular weights are used, films can undergo multiple morphological changes following film growth, which may include a reduction in height (Fig. 3a, b), formation of microparticles (Fig. 3c, d), and an increase in surface roughness. Films with lower molecular weight are more plastic than their high molecular weight counterparts; structural evolution is faster, so there is still a significant amount of solute as the bubbles reach large sizes. The combination of hypotonic pressure and the thinning of the walls lead to yielding of the film, rupture of the walls, and collapse of the film.
5) The evolution of the foam structure with development time can be visualized in a typical whitening process: optimal whiteness is reached at earlier times but fades as the foams become larger than the required range for visible Mie scattering, as shown sequentially in Fig. 1c. What is the optimal whiteness? How can it be defined or measured? And what is the required range for visible Mie scattering? They should be further defined.
6) The light scattering ability of DFP regions compare favourably with best-in-class performance in nature seen in the white scales of two species of beetles, as well as recent synthetic realizations of structural white. Is there any reference such as paper, book etc?

Combining comments (4,5,6), in revision, we have included better references to the general field of structural whiteness, as well as descriptions of how good the 'whiteness" is through the optical mean free path length l_t. Since this parameter is wavelength dependent, we compare its value at 810nm, in line with the work of peer-researchers. (Please see **Revision Text 3**). We have added this discussion to the conclusion.

The DFP process unifies diverse approaches to the modification of polymer films. Photolithography is merged with phase separation driven foam structuration resembling NIPS. It should be noted that techniques like NIPS are widely used to make highly scattering porous membranes (as reviewed[28,38]), while biomimetic approaches to highly scattering films have also been explored, characterizing both natural[7,9,39–42] and artificial[8,43–46] films with a disordered internal structure.

7) Figure 2 shows the growth and light scattering properties of DFP films. The graphs ((a) Change in thickness over time for foamed 192-kDa polystyrene films, where triangle, circle and square denote development at 22℃ (2000 J cm-2 dose), 32℃ (3000 J cm-2 dose), and 62℃ (3000 J cm-2 dose), (c) Mean diameter of 76 largest bubbles, and number of bubbles per micrometre of film width over development time for foamed 192-kDa polystyrene film, (d) Transport mean free path of 810 nm light in foamed 192-kDa polystyrene films over development time, and (inset) thickness normalized by as-illuminated film) should provide the error bar or statistical information.

Error bars have now been added; generally, statistical treatments within the paper have been improved.

8) A key feature of DFP domains is how strongly they scatter light. To gauge the light scattering ability of the films independent of their thickness, a transport mean free path (lt) at a wavelength of 810 nm from the transmission and thickness of the films was derived as shown in Fig. 2d. There is a strong reduction as the pores grow to sizes where they effectively scatter visible light, followed by an increase as they grow even larger. The reduction of opacity for long development times is also evident in Fig. 1c. As height continues to grow with time under these conditions, a similar correspondence can be seen between lt and film height. For the thin film, there are usually optical standing wave inside the film to make craze-like microfibrils like the authors did previously (Nature, 570, 363–367 (2019)). Does the similar phenomena happen in this study? If not, why not?

We differentiate a previous phenomena (Organized Microfibrillation (Nature 2019)) in revision, within our conclusion:

Solvent-induced foaming and photo-induced superficial nano-structuration in films have been reported before[47]. An optical standing wave was used to template a cross-linked, ordered porous framework in the organized microfibrillation (OM) process. By contrast DFP based foam formation depends on the partial destruction of polymers into scission fragments by UV light deep within the material (a crucial factor in achieving expanded, hierarchical structures) and where the foam dimensions are essentially only limited by the volume of material available.

9) The bubble growth kinetics underlying film expansion was considered by measuring growth exponents of the change

in film height Δh as a function of time, as shown in Fig. 2a. SEM cross-sections for the data sets are given in Extended Data Figs. 2 to 4. How was the film height measured? Was it measured for the same sample or different samples? If it was measured for the same sample sequentially, I wonder how the vacuum environment in SEM measurement affect the sample formation.

Films of the same thickness were prepared, and the expansions of each film reported at different solvent exposure times. In response to reviewer #1, #2, error bars for these thicknesses are included. Details of the SEM method have been clarified in the Methods section.

Note that in development time series, each measurement corresponds to a separate sample. Thus, heights were measured from cross-sectional SEM; given the significant scattering of light in highly foamed films, spectrophotometry is not a viable measurement tool for changes in film thickness, whilst in general, beam damage by SEM exposure is minimized in the cross-sectional analysis; the same cannot be said of beam damage/melting in FIB analysis.

10) A schematic is given in Fig. 3a, and growth height over time is given in Fig. 3b. Corresponding SEM cross-sections with thickness time series are given in Extended Data Fig. 5 to 7. Film failure begins near the top of the film, where the bubbles become largest and the walls are thinnest. This leads to bubble rupture and subsequent relaxation, which reduces the film height. How can the largest bubble and thinnest wall be predicted? Are they known only by measurement, can not be predicted?

11) The authors mentioned that with long exposure under certain conditions, microparticle formation can be seen with a brilliant iridescence, as shown in Figs. 3c, d. Figure 3a shows 'microsphere' in amorphous. Is the 'microparticle' same with the 'microsphere'?

Addressing both (10,11), and as commented in the general introduction to this response, we feel the present paper can describe the general phenomenon of the DFP process but it would require several research papers in specialized journals to individually explore the rich materials science and applications of the DFP process. Features such as iridescence are undeniably present during collapse, but ultimately the microspheres that cause this disappear, most probably into the developing solvent. In revision, we have noted their transient presence in SEM snapshots of collapse and the resulting angle independent iridescence within the supplementary section; however, we minimize speculation on how collapse induces such morphologies. (See **Revision Text 10b.**)

12) Hierarchically porous structure is a very useful material with the multiscale structure in the same material from nano to microscale. They have been used for other applications such as bioinspired radiative cooling devices (Nanoscale Horizon, 7, 1054 (2022)), energy devices (Adv. Funct. Mater., 22, 4634, (2012)), sensors, displays and etc. They can be further discussed for potential applications of the development.

Thank you for this suggestion. The versatility of DFP facilitates its realization in a range of geometries (now including 2D fibers in revision), with a high likelihood of extension to 3D colloids. This suggests that we may indeed be able to engineer hierarchical porous materials in the future. We have included the above citations in the text below.

DFP has the propensity to fit industrial deployment since it can be achieved in a wide range of polymer materials, as well as using a range of photoinitiators, and irradiation sources (Extended Data Figs. 6 and 8, and Supplementary Figs. 16 and 18). Moreover, roll-to-roll film and fiber production and in-line photochemical processing are established manufacturing routes. Versatility in geometry, particularly realizations in fibers, offer prospective routes to hierarchically porous materials[35–37].

35. Li, Y., Fu, Z. & Su, B. Hierarchically Structured Porous Materials for Energy Conversion and Storage. Adv. Funct. Mater. 22, 4634–4667 (2012).
36. Lee, J. et al. Biomimetic reconstruction of butterfly wing scale nanostructures for radiative cooling and structural coloration. Nanoscale Horiz. 7, 1054–1064 (2022).
37. Zhang, J. et al. Hierarchically Porous ZnO Architectures for Gas Sensor Application. Cryst. Growth Des. 9, 3532–3537 (2009).

13) The authors discussed that under long enough exposure and development, it was expected that the skin layer to also fail, exposing the inner structure of the foam. Combined with patternability of foam regions, this lends itself to localized modification of roughness, and thus permeability and hydrophobicity/hydrophilicity. From the observation from the authors, exposing the inner structure of the foam seems to be related to the hydrophobicity/hydrophilicity. The hydrophobicity/hydrophilicity is usually predicted by Wenzel or Cassie-Baxter model. The authors are suggested to use those models to predict the hydrophobicity/hydrophilicity.

In revision, we have measured the RMS roughness of developed films up to the point of collapse, in PS and PC ; though there is a correlation between superhydrophobicity and this roughness, but also with the existence of spiky PC microflowers ; this nanoscopic roughness adds to the hierarchical roughness present in PC, but not PS. Whilst it's a great suggestion to correlate the results to Cassie-Baxter, we prefer to push that study to a future work dedicated to maximizing the superhydrophobicity effect through a controlled understanding of the collapse process (specifically tied to the break-out crystallization dynamics that occurs), and with suitable choice of polymers and photoinitiators, to maximize this effect. **Revised Text 7** covers all of these points.

14) The foam structure, both pre- and post-collapse, becomes decorated with needle-like nanostructures protruding from bubble walls. They start isolated (Fig. 3e) but continue to grow with development time into larger features with extended needles (Fig. 3f). The function of the 'microflower' is not clear for current DFP film. Do they only affect the roughness and hydrophobicity/hydrophilicity? Are they related to other characteristics such as optical, mechanical or chemical characteristics of DFP film?

Thus far, the microflowers have only been evaluated for their impact on hydrophobicity; however, as the reviewer notes, there may be other specific applications that arise from this unique morphology. Certainly, it is expected that fiber-based materials with superhydrophobic properties could have interesting passive heating and water harvesting properties. At the time of writing, we are proceeding to explore such avenues, but the results are still too preliminary to report.

15) Exposure was also achieved using light sources with different wavelength ranges and power levels, including both monochromatic and broad-band illumination. Broad-band light sources were also effective in DFP foam formation. DFP foam formation was verified using a mercury lamp equipped with an optical filter (λi: 350-405 nm, Contact Mask Aligner, MA/BA8 Gen3, SÜSS MicroTec), and a standard LED flood lamp (λi: 395–405 nm AR-UV1-100W, Shenzhen Huanpin Testing Technology, Co., Ltd.), respectively. I wonder why monochromatic and broad-band illumination as well were effective. Does this mean the careful wavelength selection is not important for successful DFP foam formation?

That is correct, with some limitations. The wavelength needs to be in a range where the bare polymer allows enough transmittance, and the photoinitiator allows radical formation. This is key to successful sensitization of the whole film to foam formation.

16) For the practical application, scale-up manufacturing for a large area is very important. Current study was demonstrated for a relatively small area. A large-area LED array was custom-ordered from Micro Square Co., Ltd (λi : 365, 385, and 405 nm). For each wavelength, 12 × 54 bulbs were assembled in a rectangular arrangement with 1-cm spacing between bulbs along both the width and length. The irradiance of the LED array was linearly adjustable from 0 to 750 mW cm^{-2} at a working distance of 10 cm, corresponding to the range of the power adapter output. What is the limiting factor for a large area scale up? How can this limitation be overcome?

So long as a photoinitiator containing polymer material may be prepared and exposed, there is no significant limit. We have achieved patterning at standard A4 sizes (see Supplementary Fig. 17) using bar coating to replace spin coating; and the transition from this kind of coating to industrial roll-to-roll coating is something that our group is familiar with, since in the past, we have inspired a university spin-out that creates roll-to-roll CO_2 gas separation membranes (coating at levels of 30m^2/min); such products originally started as lab-based bar-coated samples. On the other hand, the power required for illumination can be increased in industrial UV systems by a factor of hundred, therefore reducing residence time within the UV reaction zone in a roll-to-roll process. As was reported in revision, control of polymer molecular weight and photoinitiator content will also significantly reduce the necessary irradiation times required for the DFP photochemical initiation, whereas development temperatures and solvents can be optimized for foaming seeds.

Moreover, there is a remarkable simplicity to this process (see Supplementary Fig. 17). The Hokusai sample created in this figure used nothing more expensive than a 30USD tanning lamp source and was a minor undergraduate student project to replace the chloroform solvent with a green solvent. In other words, we anticipate that this technology is suitable for wide scale industrial deployment.

Referee #3 (Remarks to the Author):

In their study, Easan Sivaniah and co-workers introduce deepfoam photolithography, which is a versatile strategy to locally impart porous structures within surface-near regions of thermoplastic substrates. In the presence of radical photoinitiators, the authors exploit (UV) light-mediated chain scission/crosslinking processes to change polymer-solvent interactions. Once photopatterned, the films are immersed in acetic acid acting as weak solvent and the solvent uptake leads to a volume expansion of the film. Depending on the development time and the exposure conditions, the films undergo various changes in their morphology such as a reduction in height, an increase in surface roughness or regular microparticles are formed on the samples' surface. The hierarchically structured morphologies lead to a change in optical properties and high resolution patterns with varying colors are generated. The conceptional approach is similar to a previous study of the authors (https://doi.org/10.1038/s41586-019-1299-8), which exploits solvent-induced stress crazing to form microfibrils and cavities in thermoplastic films. In the current work, they significantly advance the process by being able to create porous structures with different morphologies over varying length scales. Along with optical properties, the change in morphology also promotes a local control in surface wettability over an extended range, even reaching superhydrophic characteristics due to the hierarchical architecture of the formed structures.
From a chemistry viewpoint, the process impresses with its simplicity and might be easily extended to other light sources emitting light at longer wavelengths by adding other types of radical initiators (e.g. near IR light to activate radical initiators and generate chain scission in even deeper regions). By offering the possibility to spatially control the morphology of porous structures, the work is relevant for numerous application fields and is expected to be highly appealing for the readers of Nature. The manuscript is well written but lacks some studies on the underlying chemical mechanisms and thus, I would recommend that the manuscript requires a revision.

Major issue:
(1) The authors thoroughly studied the physical aspects of the foaming process including evolution of the porous structures and foam morphologies as a function of various parameters (e.g. exposure dose, development time, etc.). However, the chemical change (crosslinking versus chain scission) in the network has to be also addressed to better understand the foam dynamics. It's recommended that the authors include contrast curves (plotting soluble or gel fraction versus exposure dose) of the studied materials.

This issue has now been dealt with in detail, and contrast curves provided for the primary material (PS, at both molecular weights, and various THX concentrations). Please see **Revision Text 5**. In addition, ATR-FTIR, TGA, and GPC analysis is used to understand the effect of photodegradation and cross-linking of the polymer. Since the PS/THX photochemical system is in published literature already, the findings are corroborated here and a detailed report is provided as a stand-alone SI section (Supplementary Note 2), with the main conclusions written in the main text.

The primary conclusion is that indeed the relative fraction of scission products is key to foam growth dynamics and also the ultimate stability of the foam. **Reviewer #3's request proved insightful in other additional ways,** since we could qualitatively correlate the increase (upon irradiation) of scission products with an increase in the Case II diffusion front velocity.

Minor points and questions:
(2) How do mechanical or thermal properties of the thermoplastic substrates (prior to swelling) change due to the light-triggered chemical processes?

See Supplementary Note 7 for the following manuscript additions:
Preliminary characterisation was carried out on the as-cast and illuminated films, prior to development. Within error, there was no notable difference in measured film mechanical properties (via nanoindentation) before and after exposure for the longest exposures for each molecular weight studied (Supplementary Fig. 12a). Whereas one might expect the increase in scission products to soften the pre-swelled polymer film, there is sufficient cross-linked polymer to mask the difference in mechanical property. We note that TGA revealed both a loss of scission products at approximately 350 °C, with mass loss increasing with irradiation time, and an increase in crosslinked PS, as signified by a persistent tail at temperatures where un-crosslinked PS would be thermally degraded.

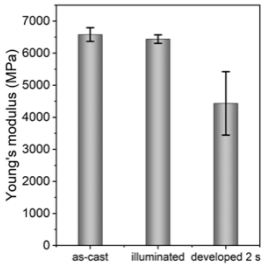

(3) How critical is the drying time of the swollen networks? How is the foam morphology affected by the evaporation kinetics of the solvent?

Please see **Revision Text 9a**. In short, the evaporation speed simply modulates the development time; the longer it takes to dry, the more the structure develops in the solvent. We have added the following to the Methods.

The samples were dried using an air blower immediately upon the completion of development (see the effect of different drying method in Supplementary Fig. 23).

(4) In the conclusion section, the authors state that foaming is possible over the entire volume. However, this is true only for very thin films. It's recommended that the authors rephrase this statement accordingly.

It is our observation that films, initially as thick as ~120 μm, are all capable of foaming due to the deep nature of the highly penetrative UV-C. This is shown in Extended Figure 1. We revise the sentence to say the following:

By contrast DFP based foam formation depends on the partial destruction of polymers into scission fragments by UV light deep within the material (a crucial factor in achieving expanded, hierarchical structures) and where the foam dimensions are essentially only limited by the volume of material available.

(5) The photoinitiator content is rather high (several experiments were carried out with films containing 9 wt% of the photoinitiator), which is expected to comprise on the penetration depth of the incident light (internal filter effect). Were the porous structures only obtained in films containing a higher photoinitiator content? If this is the case, it would be interesting to compare contrast curves of thermoplastic substrates with varying photoinitiator contents.

As recommended by the Reviewer (and presented **in Revision Text 5**), a full set of contrast curves were developed for photoinitiator contents ranging from 1 to 15%, for both low and high molecular weight polymers. The conclusion is that foaming is possible at all concentrations, whilst the dynamics and stability of the resulting foams is dependent on both Mw, photoinitiator content and irradiation energy at a given solvent development temperature.

OUR THANKS AND APOLOGIES IN ADVANCE FOR THE TIME TAKEN BY THE EDITOR AND REVIEWERS WHO MADE IT ALL THE WAY THROUGH THIS EXTENSIVE RESPONSE; WE ARE PLEASED WITH THE COLLABORATIVE ENHANCEMENTS WE COULD MAKE TO MANUSCRIPT.

For Attn of reviewers :

Thank you for your continued supportive review of our paper; we appreciate your positive responses to our revisions.

In this second revision

(1) We have made additional changes in response to reviewer #1 request for better referencing.

(2) We have understood the request of reviewer #2. The primary changes are as follows

a. We improved the following:

i. We have ensured missing exchanges between reviewers and authors are reflected in the manuscript.
ii. We enhanced the clarity of figures.

b. For the purpose of future industry usage, an extended set of technical supplementary notes are provided on **durability, resolution, scalability, materials landscape, and uniformity**. Some key points:

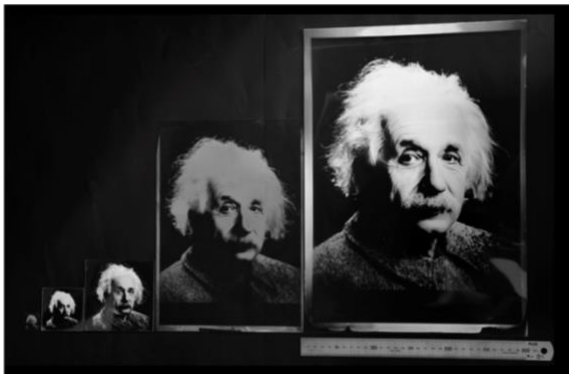

i. DFP was demonstrated at larger scales (up to A3) replacing spin-coating with a bar-coating process and lab-scale UV illumination with large area industrial-grade sources; however better industrial process control should be implemented.

ii. Resolution in DFP, as a photolithographic process, is in principle diffraction limited, but practically depends on the degree of foaming that is required, since proximal foams will physically interfere with each other. For diffractive color gratings such spacing resolution is practically ~2 microns.

iii. Details of other candidate materials and photoinitiators besides the primary ones described in the main text are now summarized.

iv. There was no indication, either through visible inspection or optical transmissivity, of significantly altered DFP print quality after 1200 cyclic bendings, or after a test of 50 heat-cold shock cycles (from ~ minus-198ºC to room temperature.

v. On the otherhand, microcracks do occur for both the foamed and original solid polymer coatings, under both types of deformations. However straightforward crack propagation in solid films appears to be stymied by the presence of the foams.

vi. All mechanical tests on DFP printing were done with a single high molecular weight of polystyrene. Such properties will change with different polymers and molecular weights or with the addition of various toughness modifiers; a detailed study and scientific discussion of DFP fracture mechanics with a wider range of industrially relevant durability tests is deferred to a future study.

These primarily technical details were added into the following supplementary notes:

Supplementary Note 09: Commentary on printing angle dependent diffractive color and its resolution limits.
Supplementary Note 11 : Preliminary evaluation of the mechanical stability of printed DFP films.
Supplementary Note 12: Commentary on the feasibility of industrial scalability and printing uniformity
Supplementary Note 13: Commentary on the use of other polymers and photoinitiators.

These additional notes are provided here, for the convenience of the reviewers, and referred to in our line-by-line responses to reviewer #2 concerning additional technical concerns.

Supplementary Note 9

Commentary on printing angle dependent diffractive color and resolution limits

Method *The resolution limit of DFP printing was studied primarily using 192-kDa polystyrene (PS) and thioxanthone (THX). 2.5-μm-thick PS films were prepared by spin-casting a solution in which thioxanthone (THX) was added at 7 wt% relative to the polymer. Unless stated otherwise, cover glass (Product code: 24241, Muto Pure Chemicals Co., Ltd.) is the substrate for casting the films. The film was illuminated either using a maskless micro-LED system or using a custom LED chamber (Thorlabs λ_i: 405 nm) with a chromium photomask. Energy dosage is 200–800 J cm^{-2}. The illuminated films were developed in acetic acid at 32 ℃.*

Ultra-high-resolution printing can be performed using a micro-LED illumination instrument (λ_i: 405 nm, Maskless Lithography Tool D-light DL-1000GS/KCH, Nano System Solutions). The micro-LED enables pixel-level control of illumination with a spatial resolution of 1 μm. The D-light DL1000 is integrated with a digital micromirror device (Texas Instruments) to regulate the projected pattern. This electromechanical system comprises 1,024 × 768 micromirrors that can be switched on or off independently. Through a lens, these mirrors direct light onto 1 μm × 1 μm regions, yielding an exposure field of 1,024 μm × 768 μm per frame. Larger patterns can be generated by stitching multiple frames together.

DFP printing in micrometer resolution can be also achieved using a chromium mask. The chromium masks were fabricated through a typical photolithographic process in a Class 100 cleanroom (Nanohub, Kyoto University). The chromium mask blank (CBL2506Bu-AZP, CST Co., Ltd) features a 100-nm thick chromium layer deposited on a 0.06-inch soda-lime glass substrate, with a proprietary photoresist coating (AZP1350, CST Co., Ltd). The chromium mask fabrication sequentially executes (1) patterning of the chromium mask blank using a microlaser (λ_i: 405 nm, DWL2000, Heidelberg Instruments), (2) development with a tetramethylammonium hydroxide (TMAH, ca. 25% in water) solution using photoresist processing equipment (KD-150CBU, Kanamex Co., Ltd.), (3) etching with a proprietary solution (S-CLEAN S-24, Sasaki Chemical Co., Ltd.), and (4) removing residual material with piranha solution in a wafer spin cleaner (KSC-150CBU, Kanamex Co., Ltd.). The as-fabricated chromium masks were verified to create feature precision as fine as one micrometer.

A graphics design system (GDS) software KLayout (version 0.28.16, https://www.klayout.de/) was used to design the patterns for printing. The software outputs the design in a binary database file format, which is then transferred to the micro-LED and microlaser lithography systems as data input. This applies to both maskless DFP and chromium mask fabrication. Color images were first converted to grayscale with luminance desaturation, then transformed into a two-tone image with Floyd–Steinberg dithering, both using GIMP software (version 2.10.36, https://www.gimp.org/). Additional details are provided in the captions of the Supplementary Figures.

Results and discussion *The micro-LED instrument allows pixel-level control of illumination with maximum printing resolution of 25,400 dots per inch (dpi) in principle. With such a microLED system, DFP demonstrates an ultrahigh printing resolution of approximately 20,000 dpi (Supplementary Fig. 18). Whereas the ultimate illumination resolution is diffraction limited and could conceivably reach higher values than 20,000 dpi, the foaming characteristic of DFP features means that adjacent foamed features can interact with each other. Hence, the printing resolution depends on the extent of development when other conditions like polymer/photoinitiator system and UV exposure are kept the same. In practice we observe that pixels set to $\geqslant$ 2 μm spacing can retain a distinct flat inter-region between two adjacently foamed features. This was demonstrated with one-dimensional (1D) gratings, consists of 1-μm-width exposed lines and 2-μm-width unexposed lines in the design. As development time increases from 95 s to 5 min (see the figure caption for experimental details), foam growth is observed for the microprinted lines, while at the same time the length of flat inter-region decreases from 1.6 μm to 0.7 μm. Increasing development time from 5 min to 2 hours observed the inter-region becomes $\leqslant$ 0.3 μm (Supplementary Fig. 19). The resolution is high enough to accurately print diffractive features for visible light. Details of designs are provided in Supplementary Fig. 20 for the DFP specimens with diffractive features and the angle-dependent colours of such a DFP specimen is demonstrated in Supplementary Fig. 21.*

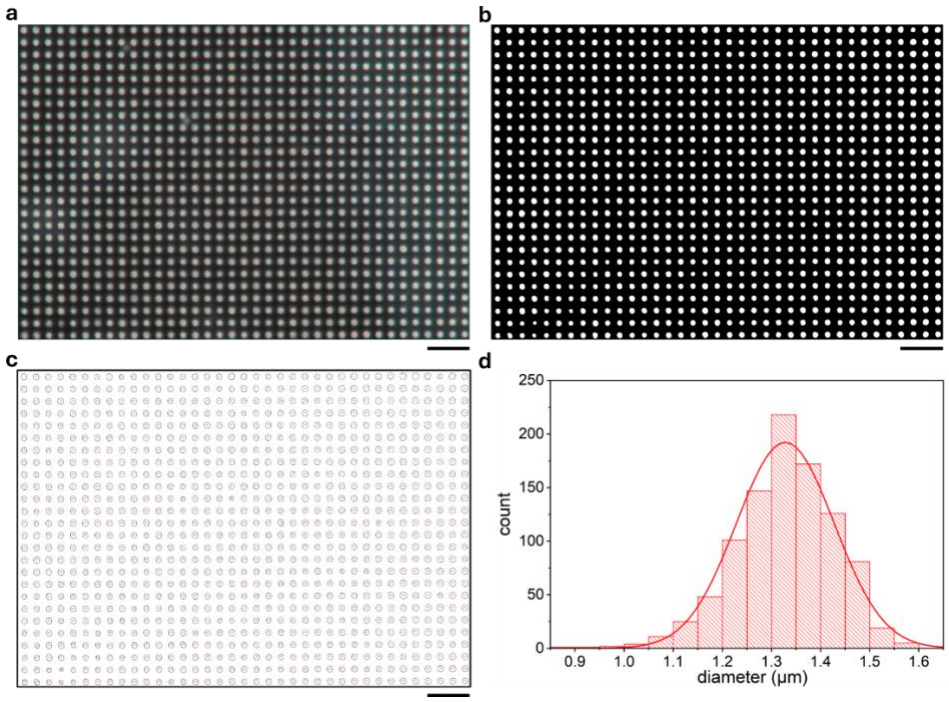

Supplementary Fig. 18 | Resolution of DFP printing. ***a****, Reflective microscopy image taken by a digital stereoscopic microscope (VHX-7000, Keyence). b, The binary image converted from (****a****) by thresholding (ImageJ).* ***c****, Pixel outlines with index labels obtained from "particle analysis" of (****b****) in ImageJ.* ***d****, Histogram of dot size distribution with a fitted normal distribution curve, $\mu \pm \sigma = 1.32 \pm 0.10$ μm ($n = 962$). Pixel size is calculated as the equivalent circular diameter from dot area (ImageJ). The mean pixel size (1.32 μm) corresponds to the resolution of 19,240 dots per inch (dpi). Scale bars, 10 μm (****a****–****c****). 2.5-μm-thick PS (192 kDa) film with 9 wt% thioxanthone content relative to PS was cast on cover glass. The film was illuminated using a microLED instrument (λ_i: 405 nm) with an energy dose of 800 J cm^{-2} and developed in 32 ℃ acetic acid. Same specimen as in Fig. 5e in the main text.*

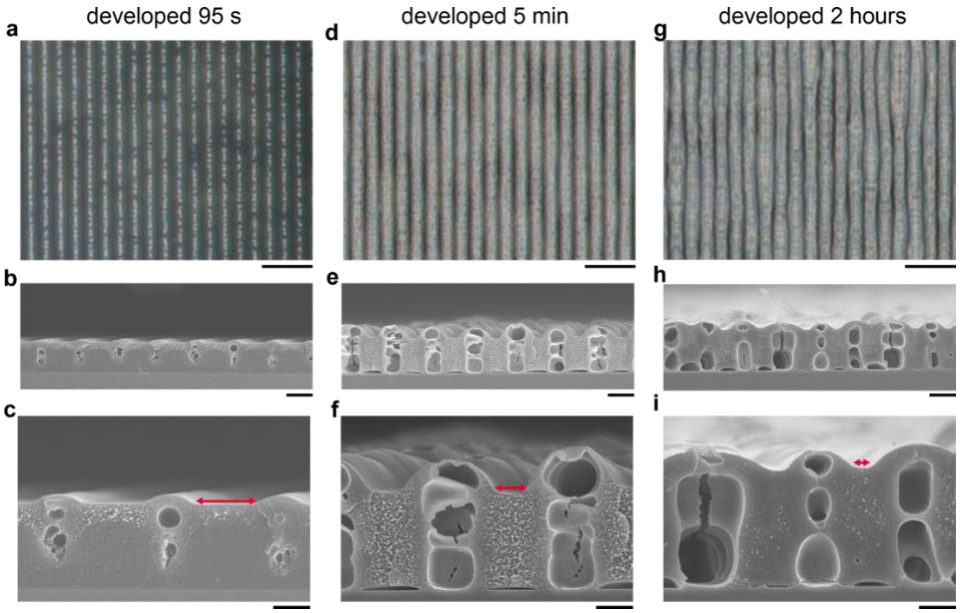

Supplementary Fig. 19 | Dependence of DFP printing resolution on development time. ***a****–****c****, Reflectance microscopy image (****a****), low- and high-magnification SEM images (****b****, ****c****) of a printed DFP film developed for 95 s.* ***d****–****f****, Reflectance microscopy image (****d****), low- and high-magnification SEM images (****e****, ****f****) of a printed DFP film developed for 5 min.* ***g****–****i****, Reflectance microscopy image (****g****), low- and high-magnification SEM images (****h****, ****i****) of a printed DFP film developed for 2 hours. Red arrows in (****c****) , (****f****) and (****i****) indicate the flat non-foamed region between two adjacently foamed regions. Scale bars, 10 μm (****a****, ****d****, ****g****); 5 μm (****b****, ****e****, ****h****); 1 μm (****c****, ****f****, ****i****). 2.5-μm-thick PS (192 kDa) film with 9 wt% thioxanthone content relative to PS was cast on cover glass. The film was illuminated using a microLED instrument (λ_i: 405 nm) with an energy dose of 750 J cm^{-2} and developed in 32 ℃ acetic acid. Design of the printing is a one-dimensional (1D) grating composed of 1-μm-width exposed lines and 2-μm-width unexposed lines.*

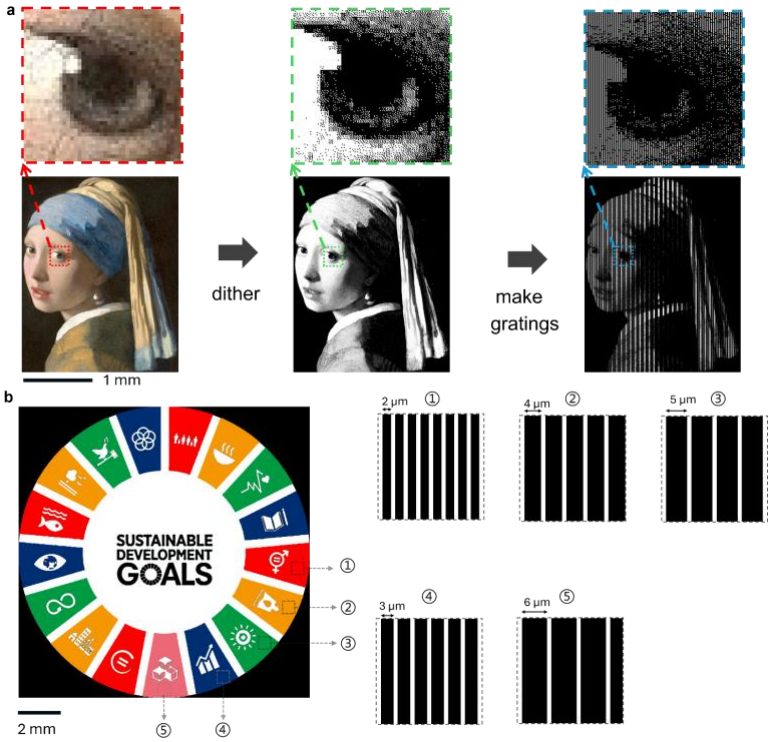

Supplementary Fig. 20 | Pattern design of the DFP specimens with diffraction-induced colors. ***a****, Pattern design of the specimen featuring diffraction-induced colours. The original colour image (Johannes Vermeer's The Gril with a Pearl Earring) is converted to a two-tone image with luminance desaturation and Floyd–Steinberg dithering, both using GIMP software (version 2.10.36, https://www.gimp.org/). The two-tone image is further intersected with a periodic grating pattern of 1-μm-width exposed lines and 2-μm-width unexposed lines to generate the final design. White and black colours denote exposed and unexposed regions, respectively. The DFP specimen is created using a microLED illumination.* ***b****, Pattern design of the specimen with both diffraction-induced colours and structural white. The design is based on the outline of the United Nations Sustainable Development Goals logo. Black and white in the design correspond to the unexposed and exposed regions, respectively. To generate diffractive colours in the sectors, one-dimensional (1D) gratings with 5 different periods are used. These are labelled with different colours in the design. In detail, the unexposed line width is 2 μm for the sectors labelled red (period ①), 4 μm for the sectors labelled yellow (period ②), 5 μm for the sectors labelled green (period ③), 3 μm for the sectors labelled blue (period ④), and 6 μm for the sectors labelled pink (period ⑤), respectively. The width of the exposed lines is 1 μm across all the sectors. A chromium photomask was made using this design. Scale bars, 1 mm (****a****); 2 mm (****b****).*

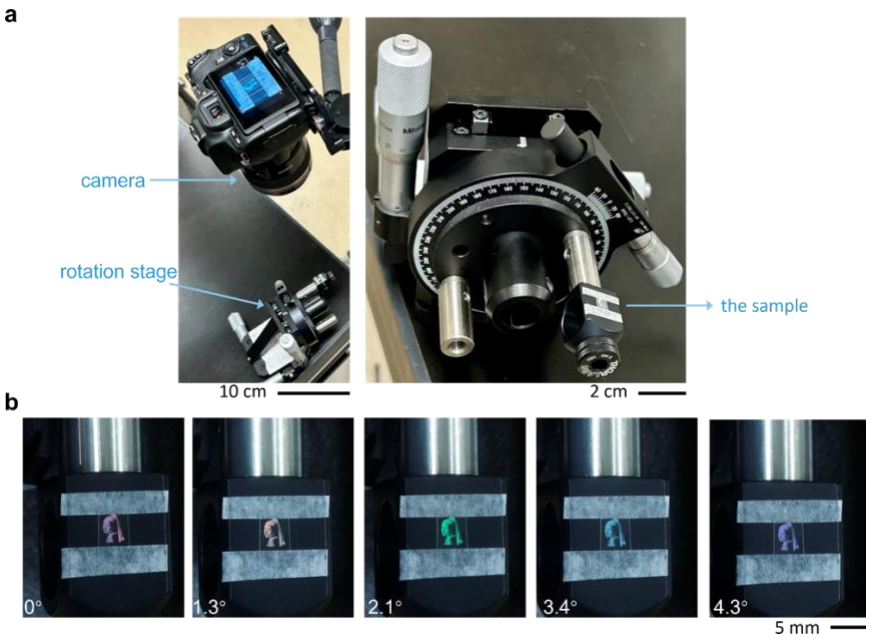

Supplementary Fig. 21 | Angle-dependent colors due to diffraction from a DFP specimen. *a, Precision rotation stage for observing diffraction-induced colours. Scale bars, 10 cm (left); 2 cm (right).* ***b****, A sequence of images was acquired at different rotation angles. The colour, arising from diffraction, continuously shifts from red to violet with increasing rotation angle. All angular values reported here are defined relative to a reference orientation. Scale bar, 5 mm. 2.5-μm-thick PS (192 kDa) film with 9 wt% thioxanthone content relative to PS was cast on PET sheet (Lumirror T60, 188-μm-thick, Toray Industries). The film was illuminated using a microLED instrument (*λ_i*: 405 nm) with an energy dose of 400 J cm*$^{-2}$ *and developed in 32℃ acetic acid.*

Supplementary Note 11

Preliminary evaluation of the mechanical stability of printed DFP films

Method

Sample preparation. *Mechanical stability of printed DFP films was evaluated by cyclic thermal shock and bending. The primary stable foam developed in this study was a 192-kDa PS film, which was printed in a decorative Mandala pattern, similar to the bending example given in Extended Data Figs. 8f, g. As for sample preparation, 2.5-μm-thick PS films were prepared by spin-casting a solution in which thioxanthone (THX) was added at 7 wt% relative to the polymer. The substrate was a PET sheet (Lumirror T60, 100-μm-thick, Toray Industries). The films were illuminated in an LED chamber (Thorlabs, λ_i: 385 nm) with an energy dose of 600 J cm-2, while an OHP mask was placed on the film for photopatterning. The illuminated films were developed in acetic acid at room temperature (22 ℃) for 1 min.*

Cyclic thermal shock. *A 36 mm × 36 mm specimen of printed DFP film was immersed in liquid nitrogen (LN_2) and held for 1 min to reach thermal equilibrium. The sample was then removed from LN_2 and exposed to ambient air (~40% RH) for 14 min to return to room temperature. During this period, surface frosting and subsequent defrosting were observed. This cycle was repeated 50 times in total, as illustrated in Supplementary Fig. 25a.*

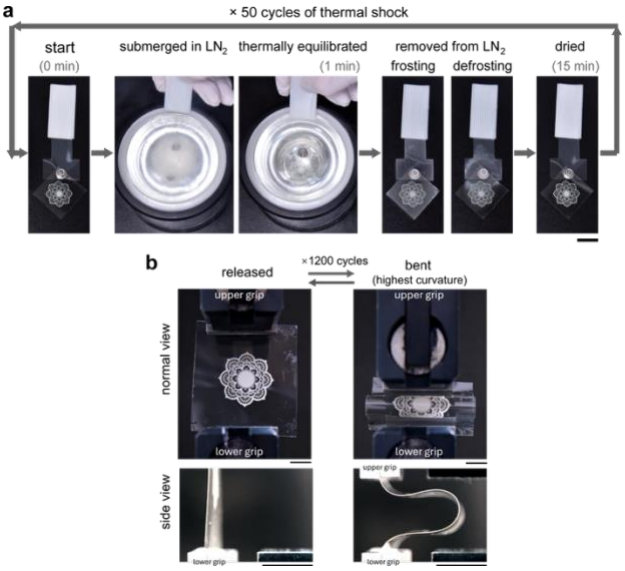

Supplementary Fig. 25 | Evaluation of mechanical stability. ***a****, Photographs showing the cyclic thermal shock using liquid nitrogen.* ***b****, Photographs showing the cyclic bending test. Scale bars, 2 cm (**a**); 1 cm (**b**).*

Cyclic bending*. A specimen of printed DFP film (50 mm × 50 mm) was clamped between two grips (5 mm clamping length at each end), with the lower grip fixed and the upper grip displaced downward by a preset displacement of 25 mm and subsequently released to impose cyclic bending deformation, using a tensile testing machine (STA-1150, Orientec Co., Ltd., Tokyo, Japan). This displacement corresponded to a maximum curvature of 0.26 mm^{-1}, while the measured maximum force reached 0.37 N. To be comparative to current literature[14] the bending test was carried out at a frequency of 7.5 cycles per minute for a total of 1200 cycles. During bending, the deformation of the film was simultaneously observed using two cameras: a DSLR camera (EOS Kiss X10, Canon) was positioned normal to the film surface, and a digital camera (XW200, Shenzhen Hayear Electronics, China) was positioned along the lateral direction to record curvature changes. The cyclic bending is demonstrated in Supplementary Fig. 25b.*

Characterization *To quantify any significant changes in the internal microstructure of the DFP film, direct transmittance spectrum was taken using a UV–Vis spectrometer (MCPD-3700, Otsuka Electronics) over different cycles of the thermal shock or bending test. The transmittance spectra were numerically integrated over the wavelength range of 320–820 nm based on the trapezoidal rule for quantitative comparison (Equations S17).*

$$I = \sum_{i=1}^{n-1} \frac{T_{D,i} + T_{D,i+1}}{2} (\lambda_{i+1} - \lambda_i) \qquad (S17)$$

where λ_i and $T_{D,i}$ denote the wavelength and corresponding direct transmittance at i-th data point, respectively, n is the total number of data points within the integration range, and I is the integrated intensity over the specified wavelength range. Relative change in the integrated intensity was evaluated by Equation S18.

$$\frac{I_j - I_0}{I_0} \times 100\% \qquad (S18)$$

where I_0 and I_j are the integrated spectral intensities of the initial state and that after j-th cyclic test of thermal shock or bending, respectively.

Surface SEM images were taken for a control printed DFP film (no bending, no thermal shock), the printed film after 50th thermal shock, and the printed film after the 1200th bending, using a JEOL JSM-7500F unit at an acceleration voltage of 5 kV. The microstructural changes in the DFP film induced by bending were also analyzed using FIB–SEM (Focused Ion Beam–Scanning Electron Microscope). Clean cross-sections of the specimen after the 1200th bending were obtained through FIB treatment. The FIB–SEM images were taken using Carl ZEISS (Crossbeam 540) under an accelerating voltage of 2.0 kV.

Results and discussion

Cyclic thermal shock. *The impact of cyclic thermal shock on the structures and properties of printed DFP film was studied at both macroscopic and microscopic levels (Supplementary Fig. 26). Overall, the printed pattern remained intact after repeated cycling of thermal shock and no discernible changes were observed at the macroscopic level, as shown in Supplementary Figs. 25a and 26a. Direct*

transmittance spectra of the foamed region were monitored over different cycles of thermal shock (Supplementary Fig. 26c). The change in the integrated intensity of direct transmittance was less than 3%, which indicates the nanostructures of the foam could be largely preserved.

For comparison purposes, a printed DFP film was prepared, and its surface was observed using SEM for both unfoamed and foamed regions, without cyclic thermal shock. Supplementary Figs. 26d show that the unfoamed region of the control DFP film is free of any cracks. Supplementary Figs. 26e show that foamed region of the control sample has characteristic surface-adjacent pores. Supplementary Fig. 26f, g reveal the impact of cyclic thermal shock on the morphology of printed DFP film at the microscopic level. Comparing the figures, cyclic thermal shock generates straight extended cracks with lengths in the unfoamed region of the film. The same cracks appear in the foamed regions, but have a more tortuous character, indicating the effect of the underlying porous foam in preventing the straight crack propagation normally seen in homogenous matter.

Cyclic bending. *The impact of cyclic bending on the structures and properties of printed DFP film was also studied at both macroscopic and microscopic levels (Supplementary Fig. 27). The intricate foamed pattern is preserved after 1200 cycles of acute bending. However, stress whitening is observed at the location of maximum curvature in the unfoamed region (label "1" in Supplementary Fig. 27a).*

Direct transmittance spectra of the foamed region were monitored over different cycles of bending (Supplementary Fig. 27b). The variation of integrated spectral intensity was less 3.5 % (Supplementary Fig. 27c), which is consistent with absence of noticeable changes in the foamed region at the macroscopic level.

SEM images reveal the impact of cyclic bending on the structures of the unfoamed and foamed DFP film at the microscopic level. As shown in Supplementary Fig. 27d, straight cracks with a spacing of ~15 μm were observed at the surface of the unfoamed region after 1200 cycles of bending, which explains the stress whitening phenomenon at the location of maximum curvature (label "1" in Supplementary Fig. 27a). A cross-section of the unfoamed film shows the thin ~2.5 μm PS film on top of the thicker 100 μm PET; note the slight scattering contrast. This upper surface was under tensile stress during bending. The cracks visible from surface SEM, are also present throughout the depth of the film. We speculate that the crack may have originated at the interface of the PET and PS surface, propagating both inwards and outwards from that point, resulting in a crack-tip at the PS film surface (Supplementary Figs. 27e, f).

In the case of foamed DFP films, SEM surface microscopy also reveals the presence of cracks (Supplementary Fig 27g), albeit with a similar diffuse and meandering appearance that was also seen in the case of thermal-shock treated samples (Supplementary Figs. 26g). In cross-section, these samples show that cracks, which may also have originated at the PS/PET interface, fail to consistently propagate to the surface, becoming pinned by the porous bubbles (Supplementary Figs. 27h, i). This incomplete crack propagation leads to the diffuse appearance of the surface SEM (Supplementary Figs. 27g).

Overall conclusion and recommendations. *Using 192-kDa polystyrene as the model, the preliminary study on mechanical stability indicates that the printed DFP pattern can be preserved after cyclic thermal shock using liquid nitrogen or acute bending. Negligible changes are observed after the cyclic tests at the macroscopic level, which is also verified by the <3.5% variation in the integrated intensity of direct transmittance. Such variances in transmittance are significantly smaller than those observed during large area coatings of DFP surfaces. However, at the microscopic level, extended cracks are formed in both unfoamed and foamed regions of the printed DFP films by cyclic thermal shock or bending. The porous structure formed by foaming is found to dull the propagation of cracks both in plane and through the thickness of the film.*

While beyond the scope of this paper, further investigation of the specific mechanisms behind crack propagation in this composite, porous system would necessitate deeper understanding of film-film interaction, internal stress distributions, and identification of the mechanisms behind failure in both materials[15,16]. A future study would also explore the phenomenon of mechanical failure in DFP foams more systematically, using multiple polymers and molecular weights, and where necessary with additives to counter any negative mechanical failures.

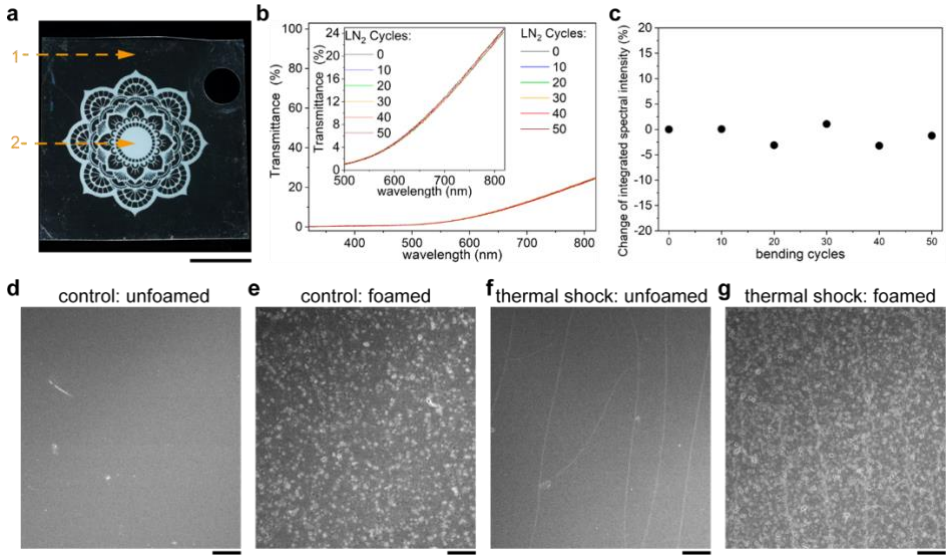

Supplementary Fig. 26 | Cyclic thermal shock. ***a****, The printed DFP film after 50 cycles of thermal shock using liquid nitrogen. The labels "1" and "2" denote the unfoamed region and foamed region, respectively, for SEM observations.* ***b****, Direct transmittance spectra over different cycles of thermal shock (inset: magnified view). The spectra were measured at the central foamed region, label "2" in (****a****).* ***c****, Relative change in the integrated intensity of direct transmittance over different cycles of thermal shock.* ***d****, Surface SEM image of the unfoamed region of a control printed DFP film.* ***e****, Surface SEM image of the foamed region of a control printed DFP film.* ***f****, Surface SEM image of the unfoamed region (label "1" in* ***a****) of the printed DFP film after 50 cycles of thermal shock.* ***g****, Surface SEM image of the foamed region (label "2" in* ***a****) of the printed DFP film after 50 cycles of thermal shock. Scale bars, 1 cm (****a****); 10 μm (****d****–****g****).*

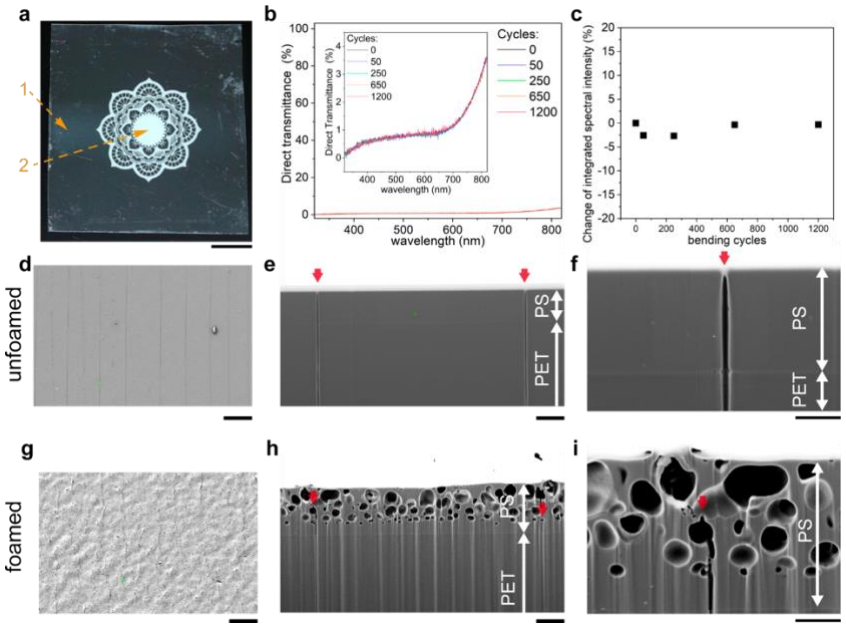

Supplementary Fig. 27 | Cyclic bending. ***a****, The printed DFP film after 1200 cycles of bending. The labels "1" and "2" denote the unfoamed region and foamed region at the location of maximum curvature, respectively, for SEM observations.* ***b****, Direct transmittance spectra over different cycles of bending (inset: magnified view). The spectra were measured at the central foamed region, label "2" in (****a****).* ***c****, Relative change in the integrated intensity of direct transmittance over different cycles of bending.* ***d****, Surface SEM image of the unfoamed region (label "1", where stress whitening is observed) after 1200 cycles of bending.* ***e****, Cross-sectional image of the unfoamed region (label "1", where stress whitening is observed) after 1200 cycles of bending, obtained by FIB-SEM.* ***f****, High magnification image of (****e****).* ***g****, Surface SEM image of the foamed region (label "2") after 1200 cycles of bending.* ***h****, Cross-sectional image of the foamed region (label "2") after 1200 cycles of bending, obtained by FIB-SEM.* ***i****, High magnification image of (****h****). Red arrow in (****e****,* ***f****,* ***h****,* ***i****) indicates an end of the extended cracks. Scale bars, 1 cm (****a****); 100 nm. 20 μm (****d****,* ***g****); 2 μm (****e****,* ***h****); 1 μm (****f****,* ***i****).*

Supplementary Note 12

Commentary on the feasibility of industrial scalability and printing uniformity

Whilst the largest films in the main figures were prepared by a batch-process method, commonly found in the semi-conductor industry, of polymer photoresist spin-coating, illumination under a physical mask, and wet-development by a solvent, we demonstrated that the DFP method can be extended to continuous printing processes.

Method. *Polystyrene (PS, 192 kDa) was primarily used for evaluating scale-up feasibility. PS was dissolved in chloroform to make 10–15 wt% solution and thioxanthone (THX) was added to the solution in the amount of 4–7 wt% relative to PS. Film coatings were performed using an RK K101 Control Coater with a No. 3 bar (24 μm wet thickness) at 2 m min^{-1}. The substrate is PET sheet (Lumirror T60, 188-μm-thick, Toray Industries, Japan) unless otherwise specified. The film was illuminated using a large LED arrary (Micro Square Co., Ltd, λ_i: 385 nm). Energy dose is in the range of 300–900 J cm^{-2} and a lower energy dosage is needed for the DFP printing with a higher THX-to-PS ratio. The illuminated film was developed in acetic acid at 32 ℃ for 1 to 10 min. The film was dried immediately upon the completion of development using an air blower bulb. Supplementary Fig. 28 shows the scale-up process. Supplementary Table 3 compares the experimental conditions between spin-cast small DFP samples and bar-coated large samples.*

Uniformity of DFP printing was studied using 192-kDa polystyrene (PS) and THX. The concentration of polystyrene solution was 9 wt%. Except for this, the other conditions for bar-coating were kept the same as mentioned above. The film was illuminated using a large LED array (Micro Square Co., Ltd, λ_i: 385 nm) with an energy dose of 150 J cm^{-2}. The illuminated film was developed in acetic acid at 32 ℃ for 1 min. For evaluating uniformity, a pattern of circular dots in A4 size was printed.

Results and Discussion *As a preliminary study on the uniformity of the DFP printing at large size, we prepared a 192-kDa polystyrene film in A4 dimensions using thioxanthone. Supplementary Fig 29a shows the printing of a chart of 8×5 circular dots, in a single, unoptimized trial. The printed whiteness is visually uniform from dots to dots throughout the A4 specimen. Moreover, we demonstrated the scaling up of DFP printing by more than an order of magnitude in area from a 2.4 cm×2.4 cm square on glass to an A3 size on PET sheet (Supplementary Fig 29b). Here, the "Einstein" photo is also a good example showing grayscale printing of DFP process: regions with stronger illumination intensity can be developed to make a more foamed structure, and hence stronger whiteness (see Fig. 5a in the main text for schematic illustration). The use of a high-power UV-A light source also reduces the illumination time from hours to minutes. Here, A3-size printing is made with polystyrene and thioxanthone, using an OHP film (0.1-mm-thick polyester film, Sakae Technical Paper Co., Ltd., Japan) as the substrate for the bar coating. More work is recommended in future to systematically optimize the experimental conditions for scale-up studies and to promote the translation of DFP technology from laboratory research to industrial-scale application.*

Table 3| Experimental conditions for making small-sized and large-sized DFP samples.

	Small-sized samples (area ⩽10 cm ×10 cm)	*Large-sized samples (area >10 cm ×10 cm)*
Substrate	*glass (primarily)*	*PET or PP sheet*
Film preparation	*Spin-casting: able to create 100 cm^2 films in 30s*	*Bar-coating: able to create A3 (~ 1260 cm^2) films in 10 s*
Illumination	*Custom LED chamber (Thorlabs, λ_i = 340, 365, 375, 385, 405 nm, power: ~0.03 W/cm^{-2} at 10 cm working distance)*	*Industrial scale, narrow bandgap LED array (Thorlabs, λ_i = 365, 385, and 405 nm, power: as high as 0.75 W/cm^{-2} at 10 cm working distance)*
Development	*Immersion in small glass dish*	*Immersion in a large tank*
Drying	*Manually, using air blower bulb*	*Manually, using an air blower bulb*

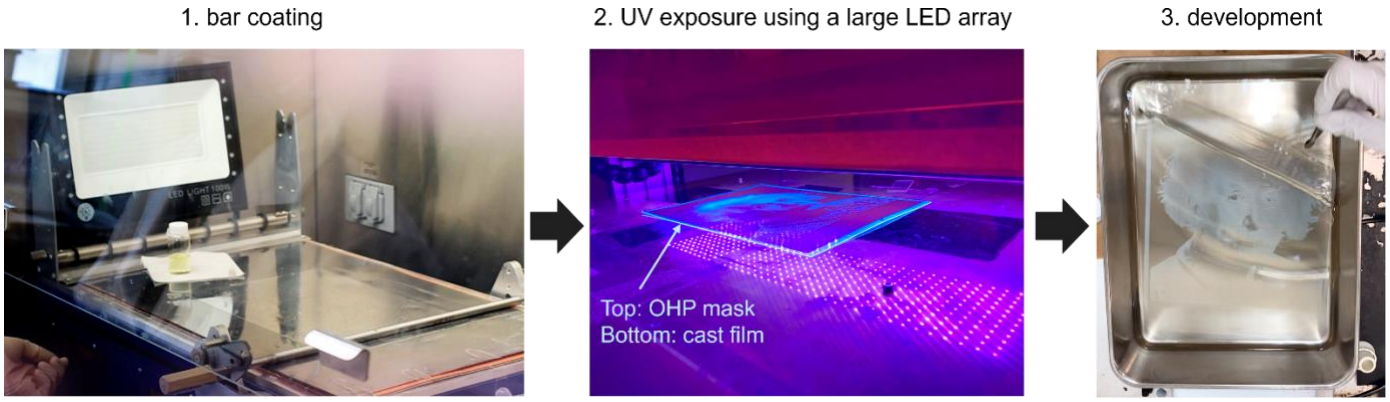

Supplementary Fig. 28 | Photographs showing the scale-up process. *Photographs from left to right: bar-coating a polymer/photoinitiator solution on A4 PET sheet (left), UV illumination using the large LED array (Micro Square Co., Ltd) (middle), and retrieving a developed DFP film from the solvent tank (right). Scale bars, 20 cm.*

Supplementary Fig. 29 | Scale-up demonstration of the DFP process and test of print uniformity. a*, Photograph of A4 printing of circular dots. Scale bar, 10 cm. The PS/THX film was illuminated using a large LED array (Micro Square Co., Ltd, , λ_i: 385 nm) with an energy dose of 150 J cm-2. The illuminated film was developed at 32℃ acetic acid for 1 min.* ***b****, Scale-up printing of the photo Albert Eistein (Original photo by Oren Jack Turner, Princeton, N.J.), where the samples* $\leqslant$ *10 cm* $\times$ *10 cm were made by spin casting and illuminated using a UV projector (λ_i: 405 nm) or using custom LED chamber (Thorlabs, λ_i: 405 or 385 nm), while the samples > 10 cm* $\times$ *10 cm were made by bar coating and illuminated using a large LED array (Micro Square Co., Ltd, , λ_i: 385 nm). The substrate for A4 and A3 specimen is 188-μm-thick PET sheet (Higashiyama Films, a subsidiary of Otsuka Chemicals, Japan) and OHP film (0.1-mm-thick polyester film, Sakae Technical Paper Co., Ltd., Japan), respectively. Ruler for scale (cm).*

Supplementary Note 13

Commentary on use of other polymers and photoinitiators

DFP is primarily demonstrated using polystyrene (PS) in this study. Mechanistic studies of DFP reveals that its formation primarily depends on plasticity of the photo-sensitized polymer, weak solvent induced phase separation, and hypotonic permeation. Photoinduced crosslinking between hydrogen abstraction–induced radical sites, and beta scission in the presence of oxygen are common mechanisms to a wide range of commercial polymers. Hence, we show that DFP process is also broadly applicable to a range of commercially available polymers (Extended Data Fig. 6). We demonstrated DFP in widely used commodity polymers including polyethylene terephthalate (PET) and poly(methyl methacrylate) (PMMA). We studied how to harness the recrystallization behaviour of polycarbonate (PC), a tough transparent engineering plastic, for patternable control of surface hydrophobicity. We also demonstrated DFP in polysulfone (PSU), a thermally and chemically stable high-performance plastic, and in cellulose triacetate (CTA), a bio-based material with high optical clarity.

We have also realized formation of DFP structures via a diverse set of photoinitiators. Thioxanthone is the primary photoinitiator studied in this paper. Apart from it, we note benzophenone and its derivatives e.g., 2-methylbenzophenone, 4,4′-bis-(diethylamino)-benzophenone, etc., anthraquinone, and phenanthrenequinone are possible for DFP processes. These photoinitiators have a broad absorption window at wavelength range of 300–400 nm. Supplementary Table 4 summarizes the polymers and photoinitiators studied in this paper.

Table 4 | Polymers and photoinitiators investigated in this study

Polymer			Photoinitiator		
	Supplier	Remarks		Supplier	Remarks
PS	Sigma Aldrich	primarily used (Figs 1–3, 5, etc.)	THX	TCI	primarily used (Figs 1a, 2–6, etc.)
PET	Tsukasa Pecto	demonstrated (Extended Data Fig. 6)	MBP	TCI	Demonstrated (Fig. 1b)
PMMA	Sigma Aldrich	demonstrated (Extended Data Fig. 6)	BP	Sigma Aldrich	For BP, BDABP, AQ, and PQ, observed DFP formation in proof-of-concept experiment with PS. Hence, note they are possible for DFP processes.
PC	Sigma Aldrich	demonstrated (Figs 4 & 6, etc.)	BDABP	Sigma Aldrich	
PSU	Sigma Aldrich	demonstrated (Extended Data Fig. 6)	AQ	TCI	
CTA	Fujifilm Wako	demonstrated (Extended Data Fig. 6)	PQ	TCI	

Note: PS denotes polystyrene, PET denotes polyethylene terephthalate, PMMA denotes poly(methyl methacrylate), PC denotes polycarbonate, PSU denotes polysulfone, CTA denotes cellulose triacetate, THX denotes thioxanthone, MBP denotes 2-methyl benzophenone, BP denotes benzophenone, BDABP denotes 4,4′-bis-(diethylamino)-benzophenone. AQ denotes anthraquinone, PQ denotes phenanthrenequinone, and TCI denotes Tokyo Chemical Industry.

Referees' comments:

Detailed explanation of revisions

Whereas all of what follows is within the paper, we explain key additional data that improve the manuscript, followed by a line-by-line response to each reviewer's comments, to address specific queries on the original manuscript. To avoid double explanations, all replies presented in this response letter primarily consist of original text (in *Times Roman, Ft 10, Italics, blue, with newly added text in purple*) from the modified manuscript. The reviewers' original comments are in (Green, Arial, Ft. 10). For the convenience of the referees, the previous reviewer's comments are attached as an appendix.

Referee #1 (Remarks to the Author):

(1) The revised manuscript presents a substantially improved and more coherent version of the original submission. The authors have clearly taken the reviewers' comments seriously and have significantly strengthened both the mechanistic understanding and the overall focus of the work.

Most importantly, the mechanistic aspects of the DFP process are now much better developed. The addition of 3D FIB-SEM analysis, confocal imaging of the solvent diffusion front, and photochemical characterization (GPC, FTIR, and TGA) provides a much clearer picture of the underlying processes governing pore nucleation, growth, and collapse. The identification of a case-II diffusion front and the discussion linking solvent permeation, chain scission, and foam formation substantially clarify the physical basis of the process - and lay the foundation for interesting followup work.

The structural characterization has also been improved, particularly through the combination of FIB-SEM analysis, optical transmittance measurements, and mechanical characterization using nanoindentation. These additions help establish a more convincing relationship between the evolving foam structure and the resulting optical and mechanical properties. The use of transport mean free path to contextualize the structural whiteness of the material relative to natural and biomimetic systems is a useful addition. It might be useful to cite the relevant literature to whiteness in discussion on page 5 a bit more.

(2) I also appreciate that the authors have streamlined the manuscript by reducing the emphasis on the microfluidic demonstrations. While I still think this aspect could be left out for a follow-up paper altogether, leaving it in like this feels ok.

All in all, a nice revision!

Many thanks – we also have added the following references to the general concept of disorder in photonics, as well as the related Mie scattering phenomenon (in the sense that whiteness indicates broadband backward Mie scattering).

10. Wiersma, D. S. Disordered photonics. Nat. Photonics 7, 188–196 (2013).

11. Miranda‐Muñoz, J. M., Lozano, G. & Míguez, H. Design and Realization of a Novel Optically Disordered Material: A Demonstration of a Mie Glass. Adv. Opt. Mater. 5, (2017).

Referee #3 (Remarks to the Author):

The authors have addressed all recommendations and questions satisfactorily. The included contrast curves at different photoinitiator concentrations have strengthened the discussion and conclusions of the work. Thus, publication of the manuscript in its current form is recommended.

Many thanks, especially for suggesting the work towards contrast curve descriptions of a foam stability phase diagram.

Referee #2 (Remarks to the Author):
(we have re-arranged the order our responses for efficient response of reviewer #2 questions that are related)

Qin and colleagues responded very well to the reviewers' comments. Even though my previous comments were really quite extensive, the authors carried out a lot of backup experiments and characterizations to successfully provide the direct evidences for the conclusion and added sound discussions. I am well satisfied with the first revision and favorable to the publication of this research results. I found that some of my previous comments are similar to the comments from other reviewers and most of them were answered satisfactorily.
Although the authors cleared up most of the important issues, there are still some remaining issues need to be addressed in further revision. To improve the quality of this research, I want to check one more review round. Here are the detailed issues needing attention,

1) Most of the discussions and new results were very useful and insightful. I am sure they will greatly strengthen the novelty of this study. However, some of them were just discussed in the rebuttal. They had better be briefly mentioned in the main manuscript or at least in the supporting information especially the new experiments and characterization requested in the first revision round.

We understand that some of reviewer exchanges were not transferred to the revised text. Notably our original responses to (14), (15), – of the reviewer #2 original questions are now paraphrased and added to suitable places in the manuscript (*see purple text below*).

Response to (14) - The function of the 'microflower' is not clear for current DFP film. Do they only affect the roughness and hydrophobicity/hydrophilicity? Are they related to other characteristics such as optical, mechanical or chemical characteristics of DFP film?

Text added :

The ability to generate superhydrophobic fabrics offers a PFAS-alternative and a potential to realize low-cost microfluidics and analysis devices[30]. Moreover, the combination of controlled optical emissivity properties of the DFP texture within a suitable composite material, printed within a fabric format, coupled to the capability to control wettability through microflower formation, could lead to passive cooling-coupled-atmospheric water harvesting resembling the natural mechanisms found in fauna and flora in arid environments [31,32].

31. Zhou, M. et al. Vapor condensation with daytime radiative cooling. Proceedings of the National Academy of Sciences 118, (2021).
32. Gurera, D. & Bhushan, B. Passive water harvesting by desert plants and animals: lessons from nature. Philosophical Transactions of the Royal Society A: Mathematical, Physical and Engineering Sciences 378, 20190444 (2020).

Response to (15) - I wonder why monochromatic and broad-band illumination as well were effective. Does this mean the careful wavelength selection is not important for successful DFP foam formation?

Text added in methods :

For the DFP process, the irradiation source wavelength must overlay with the absorption band of the photoinitiator, whilst avoiding excessive absorption by the polymer matrix. Hence, broad-band light sources were also effective in DFP foam formation. DFP foam formation was verified using an LED flood lamp (λi: 395–405 nm AR-UV1-100W, Shenzhen Huanpin Testing Technology, Co., Ltd.) and a broadband UV light source (Metal halide lamp M06-L31, Eye Cure, EYE GRAPHICS Co., Ltd., Japan).

2) The authors very well answered the reviewers' request for depth of understanding by conducting 3D analysis and photochemical analysis to clarify the dynamics and chemical driving forces behind the DFP foaming process, both during foam growth and collapse, as well as identifying the conditions whereby a foam could be stable, or collapse. And furthermore they broadened the concept of DFP by demonstrating that it could be applied equally to the 2D geometry of a fiber, generating the DFP printing of structural white and patterned wettability in fabrics. The DFP in fiber looks very interesting. However, it is still not well understood why the authors added fiber results.

Text added in main text concerning the reason for introducing fiber demonstration of DFP (*see purple text below*):

Versatility in geometry, particularly realizations in fibers, offer prospective routes to hierarchically porous materials[35–37]. Fibers form the basis of modern fabrics-based products (woven, non-woven and additive 3D-Print manufacturing), and create the opportunity to expand the functionality of DFP derived structures into a wider range of products generated by such textiles (for example non-woven masks and woven biomedical implants and other wearable technologies).

3) In response to my previous comments on case II diffusion, it is great to provide the direct evidence of a case II diffusion front of the developing solvent, acetic acid with the 3D FIB-SEM image in Figure 2a. It is also interesting to see the presence of a nucleation zone of foam behind this front, from which microphases of solvent and UV scission products nucleate and grow. However, the colors in the figure are a bit confusing cause the color is kind of randomly assigned. How about use the color according to the size of the bubbles to show the size distribution in the real FIB-SEM images?

We investigated this, and though it is a matter of individual perspective, we felt color coding by size led to difficulties to discern individual bubbles and hence their quantity, especially close to the nucleation zone. Nevertheless, the raw data of such figures will be available, should an interested reader wish to represent the data in a different way.

4) DFP is a light induced foaming process where a photosensitized polymer film is exposed to a deeply penetrating UV-A light, which initiates the production of both scission and cross-linked polymers throughout the depth of the film. A weak solvent was used to develop the DFP foam structure. The solvent permeates into the film and bubbles of solvent/scission-product rich domains are formed which nucleate, grow, and coalesce, resulting in a closed, foam-like cellular microstructure. When the UV-A light is irradiated onto the thin film, there can be light interference to form a stack of intense-weak layers. I wonder if there is any interference effect that was previously observed in reference 47 in the polymer thin film.

In Ref 47, interference was observed most easily in thin films (<1 micron) and on strongly reflective substrates (Silicon). Such interference effects were negated through removal of the conditions required for standing waves (primarily incoherence using thicker films and weak reflection substrates – glass and PET). This is stated clearly now.

Solvent-induced foaming and photo-induced superficial nano-structuration in films have been reported before[47]. An optical standing wave was used to template a cross-linked, ordered porous framework in the organized microfibrillation (OM) process. OM effects can be minimized by removing the conditions for a standing wave, such as the use of a broadband illumination system, a thicker film to ensure that light loses coherency, or minimizing reflection by using a substrate with low refractive index difference to the polymer film. By contrast DFP based foam formation depends on the partial destruction of polymers into scission fragments by UV light deep within the material (a crucial factor in achieving expanded, hierarchical structures) and where the foam dimensions are essentially only limited by the volume of material available.

6) Microfluidic fluid control usually uses inner channel for the fluid transport. However, current microfluidic uses the control of fluid flow on patterned surfaces where the effect is strong enough that a droplet passed over unexposed regions can detach small volumes from the main droplet to form isolated liquid domains (Fig. 6a, also Supplementary Movie). This may not only be applied to the controlled delivery of analytes in parallelized lab-on-a-chip applications, but also to the control of fluid flow on patterned surfaces. However, very small volumes of fluid flowing on the surface (or even closed pores that are exposed on top) will evaporate very fast. This may mean the fluidic control can not be used for the large area sample, which will not be enough useful for the microfluidic applications because the fluid properties (such as concentration, composition etc) will continuously changes and becomes unpredictable. This critical issue needs to be further discussed.

We make the following addition, noting the importance of surface conductivity and humidity control, in addition to the differential wettability, on the stability of small volumes of deposited liquids. *see text below*

The strong contrast in hydrophobicity afforded by collapsed polycarbonate DFP domains can be used to confine liquids on surfaces. This extends to surfaces exposed to liquid by different means. In Fig. 6a, a large droplet is drawn across a patterned DFP film, leaving small volumes confined to unexposed regions (see Supplementary Movie 4). The same effect is achieved via dipping (Fig. 6b); droplets readily roll off superhydrophobic regions while staying confined to less hydrophobic regions (Supplementary Fig. 21a). Colloidal suspensions may be deposited from picoliters of water in the same way, as shown in Fig. 6c and 6d, and Supplementary Fig. 22. Apart from micro-deposition of functional materials, control of vaporisation[25] through factors such as substrate conductivity and local humidity is equally important in applications that require the maintenance of liquid droplets, such as biologicals assays[26-28], and situations that benefit from enhanced evaporation such as environmental cooling[29].

25. Talbot, E. L., Berson, A., Brown, P. S. & Bain, C. D. Evaporation of picoliter droplets on surfaces with a range of wettabilities and thermal conductivities. Phys. Rev. E 85, 061604 (2012).
29. Bin Nadeem, T., Imran, M., Tandis, E. & Arshad, A. Surface engineering and nanomaterials for sustainable indirect evaporative cooling systems. npj Thermal Science and Engineering 1, 1 (2026).

Answers to the following questions are summarized in page 1 of this response, and detailed within four technical supplementary notes (10-13). Questions (5) (8) refer on **durability** under bending or thermal shock.

5) Usually, polymer thin films suffer from the crazing problem under large deformation (bending and strain). Especially, polystyrene suffers from whitening under repeated deformation. Cycling bending causes micro-structure change in polymer film. This will be very important for the actual applications. In this study, exposure is not limited to planar films. An example is shown in Fig. 5i, where a pattern has been applied to a curved poly(2-hydroxyethyl methacrylate) (PHEMA) contact lens dip-coated with polystyrene and thioxanthone. Other examples of printing on bendable substrates like polypropylene sheets are given Extended Data Fig. 8(d,e,f,g). The intricate DFP patterns are preserved after the release of acute bending. The long-term cycling acute bending test should be carried along with the cross-sectional SEM pictures to check if there is any micro/nano scale change during the bending. If there is any micro/nano scale change in the DFP film, it will change the micro structure of DFP and thus deteriorate the performance of the DFP film.

8) Usually, polymer films suffer from the poor stability at low temperature. Usually, polymer thin film becomes very brittle at low temperature and factures into pieces. Fig. 5a (in the previous paper) shows a time lapse of a DFP pattern exposed to air at reduced temperature; droplets condense selectively on unexposed, less hydrophobic regions, where they are also more prone to coalescence. I wonder if the DFP film has enough mechanical stability under low temperature.

We present a preliminary report of bending and cyclic thermal shock, where possible, mimicking studies in the academic field. The reports are primarily technical in nature, since such work is best handled in a separate study, as noted in Supplementary Note 11, citing the following references:

Overall conclusion and recommendations. *Using 192-kDa polystyrene as the model, the preliminary study on mechanical stability indicates that the printed DFP pattern can be preserved after cyclic thermal shock using liquid nitrogen or acute bending. Negligible changes are observed after the cyclic tests at the macroscopic level, which is also verified by the <3.5% variation in the integrated intensity of direct transmittance. Such variances in transmittance are significantly smaller than those observed during large area coatings of DFP surfaces. However, at the microscopic level, extended cracks are formed in both unfoamed and foamed regions of the printed DFP films by cyclic thermal shock or bending. The porous structure formed by foaming is found to dull the propagation of cracks both in plane and through the thickness of the film.*

While beyond the scope of this paper, further investigation of the specific mechanisms behind crack propagation in this composite, porous system would necessitate deeper understanding of film-film interaction, internal stress distributions, and identification of the mechanisms behind failure in both materials[15,16]. A future study would also explore the phenomenon of mechanical failure in DFP foams more systematically, using multiple polymers and molecular weights, and where necessary with additives to counter any negative mechanical failures.

Kishino, M., et al. , A. Bending Fatigue Analysis of Various Polymer Films by Real-Time Monitoring of the Radius of Curvature and Heat Generation. J. Phys. Chem. C ***127****, 14510-14517 (2023).*
Marsavina, L. & Linul, E. Fracture toughness of rigid polymeric foams: A review. Fatigue Fract. Eng. Mater. Struct. ***43****, 2483-2514 (2020).*
Thouless, M. D., et al. S. Periodic cracking of films supported on compliant substrates. J. Mech. Phys. Solids ***59****, 1927-1937 (2011).*

Questions (7) (9) refer to **resolution limits**, and diffractive color.

7) Alternatively, single “pixels” may be exposed which realize highly localized foam regions. This can be used to print dithered images with high precision. An example produced using microLED exposure is shown in Fig. 5c along with a higher magnification microscope image of the underlying dithering in Fig. 5d. SEM images of these individual foamed regions (Fig. 5e) reveals strong localization of the foaming; the resolution achieved is 20,000 dpi. What is the limiting factor for this high resolution?

9) Figure 5 f shows the angle-dependent colour of the printed image of The Girl with a Pearl Earring, placed on a human finger, printed by microLED illumination. Insets are the same sample with slight rotations. Fig. 5f shows a grating type ‘Vermeer’ image printed; tilting yields different diffractive colors. Periodic grating structures with slightly different relative spacings can be combined with structural white to create an ‘SDG’ logo specimens featuring both diffractive colour and structural whiteness. The angle information should be indicated in the picture and the scale bar is missing in this picture.

Noting that the theoretical limit is essentially diffraction limited in Supplementary Note 9, we highlight that the degree of foaming process itself will dictate the practical resolution:

Results and discussion *The micro-LED instrument allows pixel-level control of illumination with maximum printing resolution of 25,400 dots per inch (dpi) in principle. With such a microLED system, DFP demonstrates an ultrahigh printing resolution of approximately 20,000*

dpi (Supplementary Fig. 18). Whereas the ultimate illumination resolution is diffraction limited and could conceivably reach higher values than 20,000 dpi, the foaming characteristic of DFP features means that adjacent foamed features can interact with each other. Hence, the printing resolution depends on the extent of development when other conditions like polymer/photoinitiator system and UV exposure are kept the same. In practice we observe that pixels set to ≥ 2 μm spacing can retain a distinct flat inter-region between two adjacently foamed features. This was demonstrated with one-dimensional (1D) gratings, consists of 1-μm-width exposed lines and 2-μm-width unexposed lines in the design. As development time increases from 95 s to 5 min (see the figure caption for experimental details), foam growth is observed for the microprinted lines, while at the same time the length of flat inter-region decreases from 1.6 μm to 0.7 μm. Increasing development time from 5 min to 2 hours observed the inter-region becomes ≤ 0.3 μm (Supplementary Fig. 19). The resolution is high enough to accurately print diffractive features for visible light. Details of designs are provided in Supplementary Fig. 20 for the DFP specimens with diffractive features and the angle-dependent colours of such a DFP specimen is demonstrated in Supplementary Fig. 21.

Questions (10), (11) refer to **scaleability,**

10) Figure 5 shows various images generated by current technology including (b) a greyscale printing of the photo Albert Eistein using UV projector (c) printing a dithered image of the Mona Lisa by micro-LED illumination, (f) angle-dependent colour of the printed image of The Girl with a Pearl Earring, placed on a human finger, printed by microLED illumination etc. For the printing applications, this technology should be demonstrated for a large size. What is the largest size and what are the limiting factors for scale-up?

11) Continuing the previous comment, the uniformity will be prime factor for the high quality printing. How is the uniformity of the scale-up sample? The uniformity can be defined in terms of pore size, size distribution, thickness, color etc. Additionally, the discussion on the primary factor decides the uniformity and the potential solution can be further discussed.

Noting that the DFP process is essentially a photolithographic process, the basic tools for scaleup already exist in industry, but new process control parameters will need to be established. Such comments are found within Supplementary Note 12.

Results and Discussion *As a preliminary study on the uniformity of the DFP printing at large size, we prepared a 192-kDa polystyrene film in A4 dimensions using thioxanthone. Supplementary Fig 29a shows the printing of a chart of 8×5 circular dots, in a single, unoptimized trial. The printed whiteness is visually uniform from dots to dots throughout the A4 specimen. Moreover, we demonstrated the scaling up of DFP printing by more than an order of magnitude in area from a 2.4 cm×2.4 cm square on glass to an A3 size on PET sheet (Supplementary Fig 29b). Here, the "Einstein" photo is also a good example showing grayscale printing of DFP process: regions with stronger illumination intensity can be developed to make a more foamed structure, and hence stronger whiteness (see Fig. 5a in the main text for schematic illustration). The use of a high-power UV-A light source also reduces the illumination time from hours to minutes. Here, A3-size printing is made with polystyrene and thioxanthone, using an OHP film (0.1-mm-thick polyester film, Sakae Technical Paper Co., Ltd., Japan) as the substrate for the bar coating. More work is recommended in future to systematically optimize the experimental conditions for scale-up studies and to promote the translation of DFP technology from laboratory research to industrial-scale application.*

Question (15) refers to the **broadness of material choices.**

15) For the respond to previous comments on the material combination dependence, the authors carried out various backup experiment for various materials. DFP domain formation depends only on plasticity, hypotonic permeation, and crosslinking; beta scission in the presence of oxygen and crosslinking due to reaction between sites on the polymer radicalized by hydrogen abstraction are common mechanisms to a wide range of commercial polymers. Hence we show that the DFP process is also broadly applicable to a range of commercially available polymers including polycarbonate (PC) and polyethylene terephthalate (PET) using a range of photoinitiators (see Extended Data Fig 6). Besides the pictures in the extended data, if the authors can provide a table summarizing the material candidate, it will be helpful to the readers.

Such information is now found within Supplementary Note 13.

The main text briefly summarizes these contributions.

DFP has the propensity to fit industrial deployment since it can be achieved in a wide range of polymer materials, as well as using a range of photoinitiators, and irradiation sources (Extended Data Figs. 6 and 8, and Supplementary Figs. 16). Moreover, roll-to-roll film and fiber production and in-line photochemical processing are established manufacturing routes, especially within microelectronics, semiconductor and flexible printed optoelectronic industries, where the sequential steps of film casting, exposure, and development are commonly found. One primary difference of the DFP process over classic photolithography is that a mechanical foaming process replaces a chemical etching process to develop structures. Whereas this might slow down overall process times, we have shown, through a study of exposure times, photo-initiator content, polymer molecular weight, and development temperatures that such development processes are thermally, chemically and photo-energetically tunable, and can be optimized further according to specific industrial needs. A short report of various durability tests of DFP printed films including a preliminary observation of fracture modes; demonstrations of scalability (to

A3 size) and printing uniformity, and examples of material combinations are provided (Supplementary Notes 11–13 and Supplementary Figs. 25–29). Whilst such preliminary tests proved encouraging, limitations will ultimately depend on the uniformity of process control parameters of all steps at the industrial scale. Versatility in geometry, particularly realizations in fibers, offer prospective routes to hierarchically porous materials[41–43].

Industrial levels of optimization and quality control require a significantly higher degree of specialization but we hope the data provided in these three supplementary technical notes will encourage readers to consider this as a plausible industrial process in the future.

12) The mechanisms by which DFP domains scatter light, repel water, and transport fluids are all readily found in nature. White beetles remain a key benchmark for structural white, a bar met by DFP domains; water repellency by hierarchical roughness is driven by the same dewetting physics behind the lotus effect. The authors put the picture of white beetles in several pictures including Figure 1(b), Figure 3(d), Figure 5(b). However, it is a bit distractive to show them in many pictures. It can be seen in a separate figure in Figure 3(d) while the beetle in Figure 1(b), Figure 5(b) had better be removed.

The beetle (intentionally placed against a DFP background) in figure 1b, is kept since this is the first place in the manuscript where our work is related to biomimetics. Other repetitions are removed.

The evolution of the foam structure with development time can be visualized in a typical whitening process: optimal whiteness is reached at earlier times, becoming comparable to that achieved by natural benchmarks such as a white beetle, but fades as the foams become larger than the required range for visible Mie scattering[4]*, as shown sequentially in Fig. 1b.*

13) There are still some digital pictures (Extended data Figure 3) and drawings missing scale bars. They should be added to the pictures.
14) Some letters in some figures (figure 2C) are too small to read. They should be enlarged for enhanced visibility.

(13),(14) are now corrected.

Many thanks to Reviewer #2 for highlighting the need to include information that would gather interest from an industrial perspective. We hope we have now done so, though more detailed follow-up is required under more specific use-case scenarios.

For Attn of reviewers :

Thank you for your continued supportive review of our paper; we appreciate your positive responses to our revisions.

We have now received the full approval of all reviewers on the manuscript. However, as a final comment Reviewer #3 notes:

'I carefully read the responses to the comments and I found most of the issues were well addressed. Especially, the scale-up demonstration was very impressive beyond my expectation. I do not need to review this paper again but it will be great if the authors can further provide the quantitative information on the uniformity of the DFP printing especially at large size for the response to my previous comments because the scale-up may deteriorate the uniformity of the print.

I really enjoyed reading every line of this paper and now I am totally satisfied with the response from the authors and fully support the publication of this research.'

In response, while we recognize the point the reviewer makes, we feel that it would not be good practice to add additional data to a manuscript after approval. We are still at an early stage in understanding the parameters that affect print uniformity during scale-up and commercialization. For example, effects such as thermal convection within the development bath or the atmosphere, as well as during drying, are expected to cause local variations in the dynamics of the DFP processes, and must be more carefully controlled over larger print areas, to meet more exacting industry standards. Many of these parameters and their control are *likely already part of established know-how* within the printing, photography, and photolithography industries.